

# Meta-material Sensor Based Internet of Things: Design, Optimization, and Implementation

Jingzhi Hu, *Graduate Student Member, IEEE*, Hongliang Zhang, *Member, IEEE*,  
Boya Di, *Member, IEEE*, Zhu Han, *Fellow, IEEE*, H. Vincent Poor, *Life Fellow, IEEE*,  
and Lingyang Song, *Fellow, IEEE*

## Abstract

For many applications envisioned for the Internet of Things (IoT), it is expected that the sensors will have very low costs and zero power, which can be satisfied by meta-material sensor based IoT, i.e., meta-IoT. As their constituent meta-materials can reflect wireless signals with environment-sensitive reflection coefficients, meta-IoT sensors can achieve simultaneous sensing and transmission without any active modulation. However, to maximize the sensing accuracy, the structures of meta-IoT sensors need to be optimized considering their joint influence on sensing and transmission, which is challenging due to the high computational complexity in evaluating the influence, especially given a large number of sensors. In this paper, we propose a joint sensing and transmission design method for meta-IoT systems with a large number of meta-IoT sensors, which can efficiently optimize the sensing accuracy of the system. Specifically, a computationally efficient received signal model is established to evaluate the joint influence of meta-material structure on sensing and transmission. Then, a sensing algorithm based on deep unsupervised learning is designed to obtain accurate sensing results in a robust manner. Experiments with a prototype verify that the system has a higher sensitivity and a longer transmission range compared to existing designs, and can sense environmental anomalies correctly within 2 meters.

## Index Terms

Meta-materials, Internet of Things, passive sensors, unsupervised learning.

J. Hu, B. Di, and L. Song are with School of Electronics, Peking University, Beijing 100871, China (email: {jingzhi.hu, diboya, lingyang.song}@pku.edu.cn).

H. Zhang and H. V. Poor are with Department of Electrical Engineering, Princeton University, Princeton, NJ 08540 USA (email: hongliang.zhang92@gmail.com, poor@princeton.edu).

Z. Han is with Electrical and Computer Engineering Department, University of Houston, Houston, TX 77004 USA, and also with Department of Computer Science and Engineering, Kyung Hee University, Seoul 446-701, South Korea (email: hanzhu22@gmail.com).

## I. INTRODUCTION

Understanding the surrounding environments of humans and their development is of crucial importance for improving the quality of life and promoting work efficiency [1]. For this purpose, in the upcoming 6G communications, it is envisioned that an extremely large number of Internet of Things (IoT) sensors will spread to collect information of living environments, which will be approximately 10-fold more than that in 5G (10 million devices per square km) [2]. Among them, a massive number of IoT sensors will be embedded for sensing applications to monitor environmental conditions, structural integrity, and pervasive industrial processes [3]. In such sensing applications, it is required that the IoT systems with large numbers of sensors should be cost and energy efficient, easy to maintain, and environmentally sustainable [4].

To satisfy the above requirements, the IoT in 6G is expected to have sensors with extremely low cost, zero-power consumption, and no human intervention demands (e.g. recharging and maintenance) [3]. Researchers have been making constant efforts in designing low-power (LP) IoT sensors following the standards such as Zigbee, Bluetooth and its low energy extension, LoRa, and NB-IoT [5]. However, these LP IoT sensors still need power supplies like batteries to support their sensing and transmission. Though each LP IoT sensor only consumes mW level power in their active phase [6], their collective power consumption can be considerable in the massive deployment. Besides, as the battery capacity is limited, typically LP IoT sensors have a lifetime of around three to five years [7], and the periodic battery changing task leads to high maintenance costs.

Recently, various radio-frequency identification (RFID) sensors have been designed for sensing applications, which can transmit sensory data by reflecting RF signals without additional supplied power [8–9]. Nevertheless, they still require sophisticated RF energy harvesters and microchips for sensing and signal modulation, which makes their cost unable to be cheap enough for massive deployment [8]. Moreover, the microchips in the RFID sensors are likely to encounter unexpected electrical failures and breakdowns when their service time is long, especially when they are deployed in harsh environments [10]. In this case, human intervention and maintenance are also inevitable which will incur heavy tasks of finding and replacing failed sensors. As a result, current LP IoT sensors and RFID sensors are not suitable for the massive deployment in 6G IoT.

In contrast, *meta-IoT sensors*, i.e., sensors composed of meta-materials, are attractive candi-

dates for IoT sensors in 6G. The meta-IoT sensors achieve simultaneous sensing and transmission by signal reflection on metamaterial structures and are free of expensive and delicate modulation microchips and power supplies, making them significantly more cost/energy-efficient and robust. Specifically, meta-IoT sensors are composed of sub-wavelength split-ring resonator (SRR) structures that are referred to as *meta-IoT structures* and have high sensitivity towards environmental conditions. When wireless signals of a certain frequency impinge on the meta-IoT structure, the signals are reflected and become dependent on surrounding environmental conditions. Therefore, by reflecting wireless signals, the meta-IoT sensors enable environment sensing and signal transmission towards a distant receiver at the same time, and thus they follow a joint sensing and transmission working scheme.

Typically, meta-IoT sensing systems are comprised of meta-IoT sensors and wireless transceivers. In this configuration, the sensing results are obtained by the receiver using a dedicated sensing algorithm, which should consider the joint influence of sensing and transmission on the received signals. The main difference between the meta-IoT system and traditional IoT sensing systems is that it adopts metamaterial structure based passive chipless sensors. This results in that the sensing results are obtained by the receiver with received signal processing as in RF sensing systems like [11–12] rather than by the sensors themselves.

However, it remains a challenge to design an efficient meta-IoT system. *Firstly*, designing the meta-IoT structure for improving sensing accuracy is challenging. This is because it requires a computationally efficient model to capture the joint influence of the environmental conditions and the meta-IoT structure on the received signals. Such a model is difficult to establish especially in situations with larger numbers of meta-IoT sensors as expected in 6G. *Secondly*, the properties of wireless transmission, such as the multi-path effect and thermal noises, need to be considered particularly in designing the sensing algorithm. This is because, in the received signals, the influence of wireless transmission interferes with that of the environmentally sensitive reflection on the meta-IoT sensors, which makes it non-trivial for the receiver to infer the environmental conditions accurately. However, existing works lack efficient methods to optimize the structure of meta-materials and have not considered the impairments of wireless transmission in designing the sensing algorithms, which result in a limited transmission range.

To address the above challenges, we develop a joint sensing and transmission design for general meta-IoT systems with large numbers of meta-IoT sensors. We focus on the design of the meta-IoT structure and received signal processing problem since they are the main features of

meta-IoT systems. Specifically, we propose an analytical model of the received signals, which jointly considers the influence of the meta-IoT structure on the sensing and transmission for scenarios with large numbers of meta-IoT sensors. Based on this signal model, we optimize the meta-IoT structure for a general objective which is suitable for various sensing applications. Then, aiming at anomaly detection applications, we design a sensing algorithm for the system to obtain sensing results from received signal processing. The designed sensing algorithm is based on unsupervised learning and an encoder-decoder neural network, which can handle the properties of transmission such as the multi-path effect and thermal noises. Furthermore, a prototype of the designed system is implemented and tested in a typical indoor environment. In summary, the main contributions of this paper are:

- We propose a received signal model for meta-IoT structure optimization in the meta-IoT systems with a large number of meta-IoT sensors. Compared with existing works using full-wave simulation, the proposed analytical model largely reduces the computational complexity in evaluating the influence of meta-IoT structure on joint sensing and transmission.
- We design a deep unsupervised learning based sensing algorithm for meta-IoT systems. In contrast to the existing works based on direct comparison, the proposed algorithm can effectively handle the impairments due to wireless transmission and obtain accurate sensing results robustly.
- We implement a prototype of the designed system, which achieves higher sensitivity and longer transmission range compared with the existing works in a similar frequency band and having similar functions. Specifically, in a typical indoor setting, the prototype system can detect and locate temperature and humidity anomalies successfully with a range of 2 m.

The rest of the paper is organized as follows. In Section II, we discuss related work, and in Section III, we provide an overview of meta-IoT sensors. Then, in Section IV, we describe our system model and propose a received signal model. Following that, we formulate and solve the joint sensing and transmission optimization problem for meta-IoT sensors in Section V. In Section VI, we propose a sensing algorithm that is suitable for the meta-IoT systems to sense environmental anomalies. In Section VII, we present our prototype of the designed system and explain its implementation. In Section VIII, experimental results for the proposed system are provided. Finally, Section IX draws our conclusions.

## II. RELATED WORK

In this paper, we focus on meta-IoT sensing systems and their design methods. The main difference between the meta-IoT sensing systems and existing IoT systems is that meta-IoT sensing systems employ meta-IoT sensors which can perform joint sensing and transmission.

Therefore, in this section, we first review the existing works on the sensors that perform joint sensing and transmission, which are the *chipless passive sensors*. By comparing them with the meta-IoT sensors, we point out the advantages of the meta-IoT sensors and meta-IoT sensing systems. Secondly, we summarize the existing meta-material sensor based systems and discuss the inadequacies in their designs.

### A. Chipless Passive Sensors

Recently, some chipless passive wireless sensors have been proposed to sense environmental conditions, which can perform joint sensing and transmission. In [13], the authors proposed a passive wireless sensor composed of SRR circuits and a climate-sensitive polymer, which can be used to sense CO<sub>2</sub> concentration or temperature within a gas container. In [14], the authors designed a conductive-ink-based passive humidity sensor printed on a flexible Kapton film and used a focused millimeter-wave wireless transceiver to enable a long transmission range. In [15], the authors designed a chipless RFID tag to sense humidity, which is composed of a patch with slot resonators and an electric inductive-capacitive resonator. In [16], the authors also proposed a chipless RFID sensor tag for humidity monitoring, which is composed of slotted scatterer structures fabricated on the substrate of a printed circuit board.

However, traditional chipless passive sensors have larger sizes compared with their working wavelengths. Then, when multiple traditional passive sensors form a sensor array to support ubiquitous sensing applications in 6G, their unit spacing interval is larger than the working wavelength. Consider the passive sensors as antennas, and then, based on the antenna array theory [17], the array of traditional passive sensors with a larger unit spacing interval than the working wavelength has a poor concentration of reflected energy, which shortens the transmission range. As a result, without the help of expensive mmWave equipment to focus wireless signals [13] and increase the incident power, the traditional chipless passive sensors have a short transmission range.

Compared with traditional chipless passive sensors, the meta-IoT sensors are composed of densely paved meta-IoT sensor units with a smaller size than half of the working wavelength,

which provides meta-IoT sensors with two features. Firstly, it enables the meta-IoT sensors to have a larger transmission range, since their reflected signal power is more concentrated according to the antenna array theory [17]. Secondly, for a given area, a larger number of meta-IoT sensor units can be filled into the area, which indicates a higher sensitivity.

### *B. Meta-material Sensor Based Systems*

Several existing meta-material sensors have been proposed to measure physical conditions such as temperature and humidity. In [18], the authors proposed to sense temperature with an array of meta-material-based wireless sensors, and demonstrated the feasibility of wireless temperature sensing up to 200°C. In [19], the authors designed a meta-material-based sensor to sense humidity and methanol-deionized water solutions inside a waveguide testbed. In [20–21], the authors designed a general meta-material-based sensor for environmental conditions, such as temperature and humidity, and proposed an algorithm to optimize the structure of the sensors to enhance the sensing accuracy. Moreover, in [22], the authors used multiple meta-material sensors and a supervised learning algorithm to sense the distribution of environmental conditions.

Nevertheless, existing meta-material-based wireless sensing systems only consider a small number of sensors, whereas 6G demands a large or even massive number of sensors to be deployed. The methods designed for the cases with a small number of sensors cannot be extended to the cases with a large number of sensors due to the following reasons. In the small number of sensors case, the received signals can be modeled by using full-wave simulation or the summation of the reflected signals from each sensor. Besides, as the deployment scale is small, the environment around sensors can be controlled. Thus, a data set of received signals labeled with known environmental conditions can be obtained, which enables empirical comparison and supervised learning-based sensing algorithms. However, when the number of sensors is large, the received signal model in the small number of sensors case leads to high computational cost. Moreover, controlling the environment around sensors becomes infeasible, and thus an unsupervised sensing algorithm is in need.

Furthermore, existing works have not considered the impairment of wireless transmission in their system design, such as the effects of multi-paths and noises. Since both the impairments of wireless transmission and the environmentally sensitive reflection on the meta-IoT sensors impact the received signals, their mutual interference can make the receiver hard to infer the

environmental conditions correctly. To handle the above issues, an efficient sensing algorithm needs to be designed.

### III. META-IOT SENSORS

In this section, we introduce the meta-IoT sensors, which are the core component of meta-IoT systems. We first elaborate on the structure of meta-IoT sensors, and then establish a reflection coefficient model of meta-IoT sensors. By using the equivalent circuit model, the reflection coefficients of meta-IoT sensors are shown to be sensitive to environmental conditions and can be designed by changing metamaterial structures, which provides insight into meta-IoT system design.

#### A. Meta-IoT Structure

Meta-IoT sensors are based on meta-materials, which are artificial periodic structures with exotic properties that cannot be found in nature [23]. These exotic physical properties exhibited by meta-materials are underpinned by their special frequency responses. Specifically, when wireless signals impinge upon a meta-IoT sensor, its frequency response is determined by the meta-IoT structure and the conditions of surrounding environments.

A meta-IoT sensor consists of  $N_T$  units for sensing  $N_T$  different environmental conditions. Each meta-IoT unit consists of a metal SRR with a horizontal gap printed on a square supportive dielectric substrate with side-length  $l_s$  and thickness  $h_s$ . Specifically, as illustrated in Fig. 1 (a), the metal ring has the side length  $L_{\text{SRR}}$ , and its width and thickness are denoted by  $W_{\text{SRR}}$  and  $H_{\text{SRR}}$ , respectively. The gap of the SRR is of width  $d_n$  and is filled with sensitive materials, whose electric properties are sensitive to the  $n$ -th environmental condition. Due to the sensitive materials, a meta-IoT sensor's frequency response, i.e., reflection coefficients for wireless signals, are sensitive to the  $N_T$  environmental conditions.

#### B. Reflection Coefficient Model

In the following, we model the reflection coefficient of a meta-IoT sensor, which is necessary for establishing the model of received signals. Firstly, based on [13], an SRR is only excited by the RF signals having the same polarization direction as its gap direction, which means the signals with cross-polarization cannot lead to environmentally sensitive resonant absorption of SRRs. Thus, in this paper, we assume Tx and Rx antennas in the meta-IoT system to be linearly

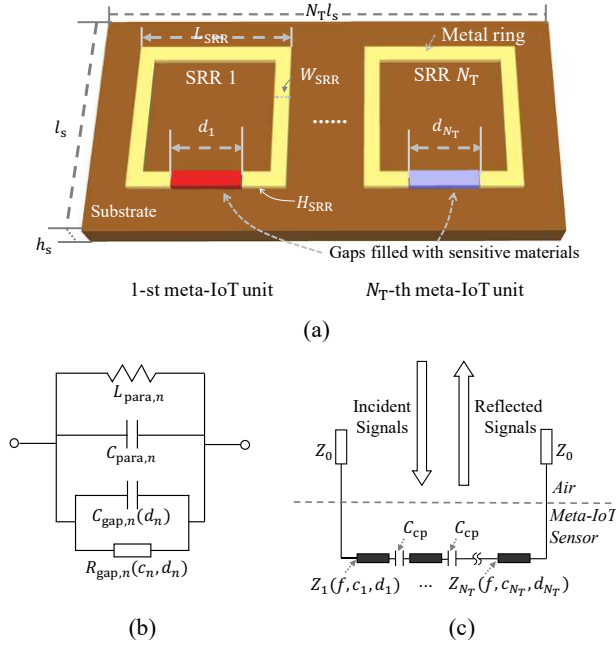


Fig. 1. (a) A meta-IoT sensor for sensing  $N_T$  environmental conditions. (b) Equivalent circuit model of the  $n$ -th meta-IoT sensor unit. (c) Equivalent circuit model of the meta-IoT sensor.

polarized and align their polarization directions with the meta-IoT sensors' gap direction. In this case, most of the incident signals on meta-IoT sensors have the electric field intensity parallel to the gap, and the signals with cross-polarization have little influence on the received signals.

Based on the transmission line theory in [24], we model the meta-IoT sensor as an equivalent load impedance connected to an equivalent transmission line of the free space, which is a commonly adopted model for meta-material particles in communication scenarios [25]. As the SRR structure of each meta-IoT unit is a resonant circuit for incident RF signals, we model the equivalent load impedance of each meta-IoT unit as an RLC resonant circuit shown in Fig. 1 (b), where R, L, and C indicate the resistance, inductance, and capacitance, respectively [26–27]. For the  $n$ -th meta-IoT unit with gap width  $d_n$ , given the  $n$ -th environmental condition being  $c_n$ , the impedance of the circuit can be calculated as

$$Z_n(f, c_n, d_n) = \left( \frac{1}{2\pi i f L_{\text{para},n}} + 2\pi i f C_{\text{para},n} + 2\pi i f C_{\text{gap},n}(d_n) + \frac{1}{R_{\text{gap},n}(c_n, d_n)} \right)^{-1}, \quad (1)$$

where  $i$  denotes the imaginary unit,  $f$  denotes the frequency of the signals, and  $L_{\text{para},n}$  and  $C_{\text{para},n}$  are the parasitic inductance and capacitance of the SRR, respectively. Besides, based



on [28], the resistance  $R_{\text{gap},n}(c_n, d_n)$  and capacity  $C_{\text{gap},n}(d_n)$  can be modeled as

$$R_{\text{gap},n}(c_n, d_n) = \frac{d_n}{\rho_{\text{mat},n}(c_n)W_{\text{SRR}}H_{\text{SRR}}}, \quad (2a)$$

$$C_{\text{gap},n}(d_n) = \hat{C}_{\text{gap},n}/d_n, \quad (2b)$$

where  $\rho_{\text{mat},n}(c_n)$  denotes the conductivity of the  $n$ -th sensitive material,  $W_{\text{SRR}}$  and  $H_{\text{SRR}}$  denote the width and thickness of each SRR, and  $\hat{C}_{\text{gap},n}$  denotes capacity of the gap with a unit width.

As shown in Fig. 1 (c), the total impedance of the meta-IoT sensor can be expressed as

$$Z(f, \mathbf{d}, \mathbf{c}) = \frac{N_T - 1}{2\pi i f \cdot C_{\text{cp}}} + \sum_{n=1}^{N_T} Z_n(f, c_n, d_n), \quad (3)$$

where  $C_{\text{cp}}$  denotes the capacity due to the coupling between adjacent meta-IoT sensor units. Besides,  $\mathbf{c} = (c_1, \dots, c_{N_T})$  denotes the environmental condition vector.

For the meta-IoT sensor, its *reflection coefficient* is a parameter that describes the fraction of the wireless signals reflected by an impedance discontinuity in the transmission medium [24]. It can be calculated by the ratio between the electric field intensities of the incident and reflected signals. Then, based on [24], the reflection coefficient can be analytically modeled by

$$\hat{\gamma}(f, \mathbf{d}, \mathbf{c}) = \frac{Z(f, \mathbf{d}, \mathbf{c}) - Z_0}{Z(f, \mathbf{d}, \mathbf{c}) + Z_0}, \quad (4)$$

where  $Z_0 = 377 \Omega$  is the characteristic impedance of the free-space transmission line.

In (2a), it can be observed that the environmental conditions determine the resistance of meta-IoT units, which influences the impedance and the reflection coefficients of the meta-IoT sensor for RF signals as shown by Eqs. (1), (3), and (4). Thus, given the received RF signals which contain the reflected signals from meta-IoT sensors, a receiver can obtain the reflection coefficients of meta-IoT sensors, based on which it can recognize the environmental conditions.

Moreover, by substituting (1)~(3) into (4), we can observe that the reflection coefficient of the meta-IoT sensor is dependent on  $\mathbf{d}$ . Therefore, the gap widths of the  $N_T$  meta-IoT units can be considered as the variables to design the meta-IoT sensor, which are thus referred to as the *meta-IoT structure vector*. Using the analytical model derived above, i.e.,  $\hat{\gamma}(f, \mathbf{d}, \mathbf{c})$ , we reveal the influence of  $\mathbf{d}$  on the reflection coefficients. Nevertheless, to obtain a precise reflection coefficient function, numerical full-wave simulation and practical experiments are in need, which is of high computational time. Therefore, to reduce the time consumption required in optimizing  $\mathbf{d}$  while ensuring the effectiveness of the results, we use  $\hat{\gamma}(f, \mathbf{d}, \mathbf{c})$  and an additional interpolation function together to fit the precise reflection coefficient function over a sampled set of  $\mathbf{d}$  denoted

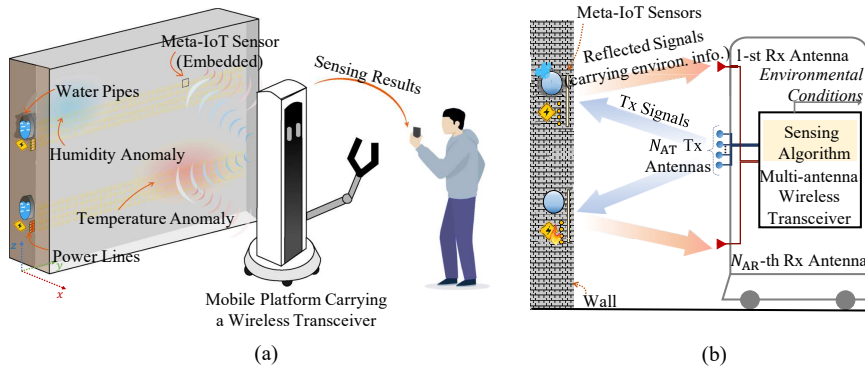


Fig. 2. (a) Illustration and (b) detailed schematic of an example of the meta-IoT system with  $N_{AR} = 2$  and  $N_{AT} = 4$ . The system is used to sense temperature and humidity in the target areas where power lines and water pipes are embedded.

by  $\hat{\mathcal{D}}_A$  as in [21]. Specifically, in this paper, we focus on the performance of meta-IoT sensors under the  $N_C$  preselected environmental conditions, which are denoted by set  $\mathcal{C}$ . Then, for each  $\mathbf{c} \in \mathcal{C}$ , the interpolation is performed in terms of  $\mathbf{d}$ , and the resulting function is denoted by  $\gamma(f, \mathbf{d}, \mathbf{c})$ , which is used in the following sections.

#### IV. SYSTEM MODEL

In this section, we describe the designed meta-IoT system, which is based on the meta-IoT sensors introduced in Section III. We first describe the system components and then propose the received signal model, where the reflection coefficients of meta-IoT sensors are based on the model established in Section III. Specifically, computationally efficient models of received signals are proposed considering the cases where the numbers of meta-IoT sensors are small and large, respectively.

##### A. System Components

The meta-IoT system is composed of two components, i.e., multiple meta-IoT sensors and a multi-antenna wireless transceiver, which can be described as follows.

1) *Meta-IoT Sensors*: The system contains  $N_{AR}$  arrays of the meta-IoT sensors. The width of each array is denoted by  $L_{MS}$ , and the center height of the  $i$ -th array is denoted by  $h_i^{MS}$ . Each meta-IoT sensor's reflection coefficients for wireless signals are sensitive to  $N_T$  different environmental conditions. The meta-IoT sensors are densely deployed along the wall and covering the areas that need to be sensed and monitored. For generality, we assume that the meta-IoT

sensors are deployed in the wall at depth  $D_w$ . This assumption is fit for both embedded scenarios where  $D_w > 0$  and the non-embedded scenarios where  $D_w = 0$ .

2) *Multi-antenna Wireless Transceiver*: The wireless transceiver contains a Tx antenna array with  $N_{AT}$  antennas,  $N_{AR}$  Rx antenna, and a signal processor. The center height of the Tx antenna array is denoted by  $h_c^{AT}$ , and the interval spacing between Tx antennas is  $\delta^{AT}$ . All the Tx and Rx antennas are directional with main lobes horizontally orientated towards the wall. Through the Tx antennas, signals within frequency band  $[f_{lb}, f_{ub}]$  are transmitted towards the  $N_{AR}$  meta-IoT sensor arrays. Then, the  $N_{AR}$  Rx antennas measure the received signals, based on which the signal processor uses a *sensing algorithm* to estimate the environmental conditions. Moreover, the wireless transceiver is installed on a mobile platform, such as a home-service robot or a UAV [29], which can move to sense the environmental conditions at different locations. An example of a meta-IoT system with  $N_{AR} = 2$  and  $N_{AT} = 4$  is depicted in Figs. 2 (a) and (b), which is used for sensing temperature and humidity inside buildings. As shown in Fig. 2 (a), the meta-IoT sensors are embedded inside the building and covering some target sensing areas (e.g., the areas where power lines and water pipes are embedded). At a certain location shown in Fig. 2 (b), the wireless transceiver transmits signals that are reflected back by the meta-IoT sensors and carrying the information of the environmental conditions. By handling the received reflected signals with its sensing algorithm, the wireless transceiver can estimate the environmental conditions at different locations and provide sensing services for the users, e.g., anomaly detection and localization.

Moreover, as shown in Fig. 2 (b), the heights of the Rx antennas and the Tx antenna array are set symmetrical with respect to the height of the meta-IoT sensor arrays. This is because for the wireless signals with wavelength larger than the spacing interval of meta-IoT sensor unit, the meta-IoT sensor arrays is equivalent to a uniform medium like a mirror. Then, the signal reflection angle on the meta-IoT sensor arrays is approximately equal to the incident angle.

Furthermore, the multi-antenna wireless transceiver is able to move horizontally along the wall to measure the meta-IoT sensors at different locations. The mobile platform moves along the  $y$ -axis to scan the meta-IoT sensors at different locations, keeping with measuring distance  $D$ . Specifically, it moves to  $N_{loc}$  different measurement locations, and uses the wireless transceiver to measure the reflected signals of meta-IoT sensors at each location.

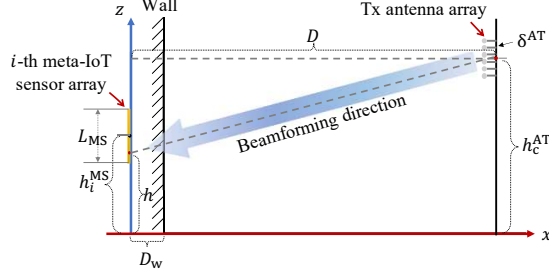


Fig. 3. Vertical section of the meta-IoT system, where the Tx antenna array aims its beam towards the meta-IoT sensors at height  $h$  in the  $i$ -th meta-IoT sensor array.

### B. Received Signal Model

In the following, we propose the analytical received signal model for the meta-IoT system, jointly considering the influence of sensing and transmission. To facilitate analysis, we use the beamforming capability of the Tx antenna array so that the transmitted signal beam is aimed at the  $i$ -th meta-IoT sensor array when measuring it. Without loss of generality, we assume that the Tx beamforming is performed by the Tx antennas adding additional phases to their transmitted signals, and the beam is aimed at the meta-IoT sensors at height  $h$ , as shown in Fig. 3.

Specifically, we focus on modeling the received signals due to the reflection of meta-IoT sensor arrays, which contain information on environmental conditions. By modeling this part of received signals, we facilitate the formulation of the optimization problem for the meta-IoT system's sensing performance. Other arriving signals at the receiver, such as the reflected signals from the walls, are omitted since they are not sensitive to environmental conditions and cannot contribute to the sensing performance of the meta-IoT system.

Based on the transmission model of metamaterial surfaces proposed and experimentally verified in [30], the influence of metamaterial particles on normal and oblique incident signals can be approximated by a reflection coefficient multiplied by a normalized radiation pattern factor. Since the SRR-based meta-IoT sensor has a radiation pattern close to a hemisphere, its normalized radiation pattern can be approximated by 1, and thus its influence on the signal transmission can be modeled by the reflection coefficient in (4). Thus, the signals transmitted by the  $j$ -th Tx antenna, reflected by the  $i$ -th meta-IoT sensor array, and received by the  $i$ -th Rx antenna can be expressed as

$$y_{j,i}(f, \mathbf{d}, \mathbf{c}, h, D) = \iint_{\mathbf{x}^M \in \mathcal{S}_i^M} \sqrt{P} \cdot g_j^{\text{Tx}}(\mathbf{x}_j^{\text{Tx}}, \mathbf{x}^M, f, h, D)$$

$$\cdot \gamma(\mathbf{x}^M, f, \mathbf{d}, \mathbf{c}) \cdot g_i^{\text{Rx}}(\mathbf{x}_i^{\text{Rx}}, \mathbf{x}^M, f, D) \cdot d\mathbf{x}^M. \quad (5)$$

In (5), the surface integral is over the surface of the  $i$ -th meta-IoT sensor array, which is denoted by  $\mathcal{S}_i^M$ , and the differential on the surface is denoted by  $\mathbf{x}^M$ . In the surface integral, the first term, i.e.,  $\sqrt{P}$  is the magnitude of the Tx signal with  $P$  being the Tx power. The second term, i.e.,  $g_j^{\text{Tx}}(\mathbf{x}_j^{\text{Tx}}, \mathbf{x}^M, f, h, D)$ , indicates the channel gain from the  $j$ -th Tx antenna at  $\mathbf{x}_j^{\text{Tx}}$  to  $\mathbf{x}^M$ . The third term, i.e.,  $\gamma(\mathbf{x}^M, f, \mathbf{d}, \mathbf{c})$  is the reflection coefficient of the meta-IoT sensor at  $\mathbf{x}^M$ , which is modeled based on (4). The reflection coefficient indicates the magnitude ratio and phase shift between the reflected and incident RF signals [24]. Thus, the product of the first three terms represents the reflected RF signals of the meta-IoT sensor at  $\mathbf{x}^M$ , and the magnitude of the scattering RF signals can be calculated by  $\sqrt{P} \cdot |g_j^{\text{Tx}}(\mathbf{x}_j^{\text{Tx}}, \mathbf{x}^M, f, h, D) \cdot \gamma(\mathbf{x}^M, f, \mathbf{d}, \mathbf{c})|$ . The fourth term, i.e.,  $g_i^{\text{Rx}}(\mathbf{x}_i^{\text{Rx}}, \mathbf{x}^M, f, D)$ , indicates the channel gain from  $\mathbf{x}^M$  to the  $i$ -th Rx antenna at  $\mathbf{x}_i^{\text{Rx}}$ . Specifically, the second and fourth terms in (5) can be expressed by

$$g_j^{\text{Tx}}(\mathbf{x}_j^{\text{Tx}}, \mathbf{x}^M, f, h, D) = g_j^{\text{Tx}}(f, \theta_{j,i}^{\text{Tx}}) \cdot e^{i\varphi_{j,i}^{\text{Tx}}(f, h, D)} \cdot g(\mathbf{x}_j^{\text{Tx}}, \mathbf{x}^M, f, D), \quad (6)$$

$$g_i^{\text{Rx}}(\mathbf{x}_i^{\text{Rx}}, \mathbf{x}^M, f, D) = g_i^{\text{Rx}}(f, \theta_i^{\text{Rx}}) \cdot g(\mathbf{x}_i^{\text{Rx}}, \mathbf{x}^M, f, D), \quad (7)$$

where  $\varphi_{j,i}^{\text{Tx}}(f, h, D)$  is the added phase to the signals of frequency  $f$  transmitted by the  $j$ -th Tx antenna for beamforming when measuring the  $i$ -th meta-IoT sensor array at height  $h$  and distance  $D$ , and  $g_j^{\text{Tx}}(f, \theta_{j,i}^{\text{Tx}})$  and  $g_i^{\text{Rx}}(f, \theta_i^{\text{Rx}})$  indicate the gains of the  $j$ -th Tx antenna and the  $i$ -th Rx antenna, respectively. Here,  $\theta_{j,i}^{\text{Tx}}$  denotes the emission angle of the signals from the  $j$ -th Tx antenna to the  $i$ -th meta-IoT sensor array, and  $\theta_i^{\text{Rx}}$  denotes the incident angle of signals from the  $i$ -th meta-IoT sensor array to the  $i$ -th Rx antenna, which can be approximated by

$$\theta_{j,i}^{\text{Tx}} = \arctan\left(\frac{h_j^{\text{Tx}} - h_i^{\text{MS}}}{D}\right), \quad \theta_i^{\text{Rx}} = \arctan\left(\frac{h_i^{\text{MS}} - h_i^{\text{Rx}}}{D}\right), \quad (8)$$

where  $h_j^{\text{Tx}}$ ,  $h_i^{\text{MS}}$ , and  $h_i^{\text{Rx}}$  denote the heights of the  $j$ -th Tx antenna, the center of the  $i$ -th meta-IoT sensor array, and the  $i$ -th Rx antenna, respectively.

Furthermore,  $g(\mathbf{x}, \mathbf{x}^M, f, D)$  in (6) and (7) indicates the propagation channel gain from  $\mathbf{x}$  to  $\mathbf{x}^M$ , which can be calculated by

$$g(\mathbf{x}, \mathbf{x}^M, f, D) = \underbrace{\frac{ve^{-i\frac{2\pi f}{v}\|\mathbf{x}-\mathbf{x}^M\|}}{4\pi f\|\mathbf{x}-\mathbf{x}^M\|}}_{\text{Free-space propagation}} \cdot \underbrace{e^{-\beta\frac{D_w}{D}\|\mathbf{x}-\mathbf{x}^M\| - i\frac{2\pi f D_w}{vD}(n_w-1)\cdot\|\mathbf{x}-\mathbf{x}^M\|}}_{\text{In-wall propagation}}, \quad (9)$$

where  $v$  denotes the speed of light.

In (9), the first term is derived from the signal propagation in free-space, and the second term is the factor accounting for the in-wall propagation. Besides,  $\beta$ ,  $n_w$ , and  $D_w$  denote the attenuation factor, the relative refraction index, and the thickness of the wall, respectively. Moreover, in (6),  $\varphi_{j,i}^{\text{Tx}}(f, h, D)$  aligns the phases of the transmitted signals of the  $N_{\text{AT}}$  antennas in the direction towards the  $i$ -th meta-IoT sensor array at height  $h$ .

Nevertheless, due to the integration in (5), the channel model is hard to calculate, which results in difficulty when designing the meta-IoT structure and setting the added phase for beamforming. To handle this issue, in the following, we provide computationally efficient models of received signals considering the cases where the numbers of meta-IoT sensors are small and large, respectively.

1) *Small number of meta-IoT sensors case:* As the size of each meta-IoT sensor is on the sub-wavelength scale, the variation of the wave propagation distance and arriving phase across the region of a meta-IoT sensor is negligible [31]. Therefore, we can simplify the integration in (5) by discretizing it into a summation, which can be expressed as

$$y_{j,i}^{\text{small}}(f, \mathbf{d}, \mathbf{c}, h, D) \approx \sqrt{P} \cdot \sum_{m \in \mathcal{N}_i^{\text{M}}} g(\mathbf{x}_j^{\text{Tx}}, \mathbf{x}_m^{\text{M}}, f, D) \cdot e^{i\varphi_{j,i}^{\text{Tx}}(f, h, D)} \cdot \gamma(f, \mathbf{d}, \mathbf{c}) \cdot g(\mathbf{x}_i^{\text{Rx}}, \mathbf{x}_m^{\text{M}}, f, D) \cdot A, \quad (10)$$

where  $A = N_{\text{T}} l_{\text{s}}^2$  is the area of a meta-IoT sensor and  $\mathcal{N}_i^{\text{M}}$  denotes index set of the meta-IoT sensors in the  $i$ -th array,  $\mathbf{x}_m^{\text{M}}$  is the coordinate of the center of the  $m$ -th meta-IoT sensor.

Equation (10) is accurate and computational efficient when the number of meta-IoT sensors is small. Nevertheless, (10) is not fit the case whose number of meta-IoT sensors is large as the summation still incurs high computation complexity.

2) *Large number of meta-IoT sensors case:* As expected in 6G communications, the sensors should be massively deployed to support ubiquitous sensing. Therefore, it is both necessary and important to obtain a computationally efficient received signal model for cases where large numbers of meta-IoT sensors are deployed. Thanks to the effective medium property of the meta-materials, we can consider the meta-IoT sensor array with a large number of meta-IoT sensors as a uniform reflective surface. Thus, the reflection of the wireless signals on a meta-IoT sensor array is similar to the reflection of light on a uniform surface. Therefore, we can obtain a much simplified received signal model by the following proposition.

**Proposition 1:** Assume that the  $i$ -th meta-IoT sensor array is electrically large, i.e., both its length and width are sufficiently larger than the wavelength  $\lambda = v/f$  of the incident signals. Then, the received signal of the  $i$ -th Rx antenna for the signals transmitted by the  $j$ -th Tx antenna and reflected by the  $i$ -th meta-IoT sensor array can be approximated by

$$y_{j,i}^{\text{large}}(f, \mathbf{d}, \mathbf{c}, h, D) \approx \sqrt{P} \cdot g_j^{\text{Tx}}(f, \theta_{j,i}^{\text{Tx}}) \cdot e^{i\varphi_{j,i}^{\text{Tx}}(f, h, D)} \cdot g_i^{\text{Rx}}(f, \theta_i^{\text{Rx}}) \cdot \chi(f, \mathbf{d}, \mathbf{c}, D) \cdot g_{\text{sr}}(\mathbf{x}_i^{\text{Rx}}, \mathbf{x}_j^{\text{Tx}}, f, D), \quad (11)$$

where  $\chi(f, \mathbf{d}, \mathbf{c}, D)$  is a coefficient due to the reflection on the meta-IoT sensor array, and  $g_{\text{sr}}(\mathbf{x}_i^{\text{Rx}}, \mathbf{x}_j^{\text{Tx}}, f, D)$  is the gain of the specular reflection path from  $\mathbf{x}_j^{\text{Tx}}$  to  $\mathbf{x}_i^{\text{Rx}}$ , i.e.,

$$g_{\text{sr}}(\mathbf{x}_i^{\text{Rx}}, \mathbf{x}_j^{\text{Tx}}, f, D) = \frac{v e^{-i\frac{2\pi f}{v}\|\tilde{\mathbf{x}}_i^{\text{Rx}} - \mathbf{x}_j^{\text{Tx}}\|}}{4\pi f \|\tilde{\mathbf{x}}_i^{\text{Rx}} - \mathbf{x}_j^{\text{Tx}}\|} \cdot e^{-\beta\frac{D_w}{D}\|\tilde{\mathbf{x}}_i^{\text{Rx}} - \mathbf{x}_j^{\text{Tx}}\| - i\frac{2\pi f D_w}{vD}(n_w - 1)\|\tilde{\mathbf{x}}_i^{\text{Rx}} - \mathbf{x}_j^{\text{Tx}}\|}, \quad (12)$$

where  $\tilde{\mathbf{x}}_i^{\text{Rx}}$  is the symmetric point of  $\mathbf{x}_i^{\text{Rx}}$  with respect to the surface of meta-IoT sensor arrays. Besides,  $\chi(f, \mathbf{d}, \mathbf{c}, D)$  can be calculated by

$$\chi(f, \mathbf{d}, \mathbf{c}, D) = \frac{Dv^2\gamma(f, \mathbf{d}, \mathbf{c})}{2\beta D_w v f + 4\pi f^2 i(D + D_w(n_w - 1))}. \quad (13)$$

*Proof:* See Appendix A. ■

As the number of meta-IoT sensors in the considered system is large, we adopt the received signal model (11) in this paper. Without loss of generality, we assume that the received signals are measured at  $N_F$  frequencies, which is denoted by set  $\mathcal{F}$ . Consequently, based on (11) the received signal vector of the  $i$ -th Rx antenna is can be denoted by

$$\mathbf{y}_i(\mathbf{d}, \mathbf{c}, h, D) = \sum_{j=1}^{N_{\text{AT}}} (y_{j,i}^{\text{large}}(f_1, \mathbf{d}, \mathbf{c}, h, D), \dots, y_{j,i}^{\text{large}}(f_{N_F}, \mathbf{d}, \mathbf{c}, h, D)). \quad (14)$$

Moreover, based on (12), to align the phase of the received signals when different Tx antennas are transmitting, the added phase for beamforming in (10) can be set to

$$\varphi_{j,i}^{\text{Tx}}(f, h, D) = \left(\frac{2\pi f}{v} + \frac{2\pi f D_w}{vD}(n_w - 1)\right) \cdot (\|\mathbf{x}_j^{\text{Tx}} - \tilde{\mathbf{x}}_i^{\text{Rx}}\| - \|\mathbf{x}_1^{\text{Tx}} - \tilde{\mathbf{x}}_i^{\text{Rx}}\|). \quad (15)$$

Given that  $D \gg \delta^{\text{AT}}$  and  $D \gg D_w$ , the above equation can be approximated by

$$\varphi_{j,i}^{\text{Tx}}(f, h, D) \approx -\frac{(j-1) \cdot 2\pi f \delta^{\text{AT}}}{v} \cdot \frac{h - h_c^{\text{AT}}}{\sqrt{D^2 + (h - h_c^{\text{AT}})^2}}, h \in [h_i^{\text{MS}} - L_{\text{MS}}/2, h_i^{\text{MS}} + L_{\text{MS}}/2], \quad (16)$$

where  $h_c^{\text{AT}}$  denotes the center height of the Tx antenna array,  $\delta^{\text{AT}}$  is the interval between adjacent Tx antennas, and  $L_{\text{MS}} = N_{\text{MS}} \cdot l_s$  denotes the vertical length of a meta-IoT sensor array with  $N_{\text{MS}}$  being the number of sensors in a column.

**Computational complexity analysis:** The complexity of calculating the  $N_F$ -dimensional received signal vectors of the  $N_{AR}$  meta-IoT sensor arrays by (14) can be analyzed as follows. To calculate the  $N_F$ -dimensional received signal vectors of the  $N_{AR}$  meta-IoT sensor arrays, Eq. (11) needs to be calculated for  $N_F N_{AT} N_{AR}$  times. As for Eq. (11), its computational complexity is in proportion to that of reflection coefficient  $\gamma(f, \mathbf{d}, \mathbf{c})$ , which is calculated by Eqs. (3) and (4). Based on Eq. (3), the calculation of  $\gamma(f, \mathbf{d}, \mathbf{c})$  has the complexity of  $\mathcal{O}(N_T)$ . Therefore, in summary, the computational complexity of all the received signal vectors is  $\mathcal{O}(N_T N_F N_{AT} N_{AR})$ .

In contrast, if the received signal model for the small number of meta-IoT sensors case is adopted, then based on (10) and the above analyses, the computational complexity of all the received signal vectors is  $\mathcal{O}(N_M N_T N_F N_{AT} N_{AR})$ , where  $N_M$  denotes the number of meta-IoT sensors in a meta-IoT sensor array.

It can be observed that the computational complexity of using the received signal model for the small number of sensors case is  $N_M$  times higher than using that for the large number of sensors case. Since  $N_M$  is large in the considered scenarios, then using Eq. (11) rather than (10) for the calculation of received signals can efficiently reduce the computational complexity.

## V. JOINT SENSING AND TRANSMISSION OPTIMIZATION FOR META-IOT STRUCTURE

In this section, we first formulate the meta-IoT structure optimization problem of the meta-IoT system in Section V-A. For generality, we consider the objective to maximize the discernibility of received signals under different environmental conditions, which is suitable for various sensing applications. Then, an efficient meta-IoT structure optimization algorithm is proposed in Section V-B.

### A. Problem Formulation

Before formulating the optimization problem of the meta-IoT structure, we first specify the feature vectors obtained from the received signals, which are used to evaluate the environmental conditions. For the sake of feasibility of the meta-IoT system, we take the amplitude of the received signals to obtain the sensing results since the measurement of signal amplitude is generally easier than that of the signal phase, which requires less sophisticated equipments. Besides, to magnify the difference between small signal amplitudes, we use decibel measure instead of decimal measure. Moreover, for each meta-IoT sensor array, multiple heights are taken into consideration in the Tx beamforming, which is denoted by a *height displacement set*



$\mathcal{S}_{\text{dH}} = \{\Delta h_m = -L_{\text{MS}}/2 + (m - 1) \cdot L_{\text{MS}}/N_{\text{dH}} | m \in [1, N_{\text{dH}}]\}$  with  $|\mathcal{S}_{\text{dH}}| = N_{\text{dH}}$ . Furthermore, assume that the wireless transceiver has  $N_{\text{MD}}$  different potential measuring distances, which is denoted by  $D_q$  ( $q \in [1, N_{\text{MD}}]$ ). Therefore, given environmental condition  $\mathbf{c}$  and a certain measurement location, the *feature vector* to obtain the sensing result for the  $i$ -th meta-IoT sensor array can be expressed as

$$\mathbf{p}_{i,m}(\mathbf{c}; \mathbf{d}, D_q) = 10 \log(|\mathbf{y}_i(\mathbf{d}, \mathbf{c}, h_i^{\text{MS}} + \Delta h_m, D_q)|), i \in [1, N_{\text{AR}}], m \in [1, N_{\text{dH}}], q \in [1, N_{\text{MD}}]. \quad (17)$$

Then, based on (17), the formulation of meta-IoT structure optimization can be described as follow. Without loss of generality, we consider the sensing algorithm to infer environmental conditions from the received signals as a general classification algorithm. To ensure classification accuracy, it demands the received reflected signals under different environmental conditions to be as *discernible* as possible.

Consider  $\mathbf{g}^w$  as a general classification function, which infers the environmental condition vector corresponding to a feature vector, and thus we need to maximize the *discernibility* of the feature vectors for different environmental conditions in order to maximize the classification performance. One of the widely adopted discernibility measures is the Euclidean distance, which is used to evaluate the distance between two vectors and indicates how much two vectors can be discerned from each other [32]. Intuitively, a smaller Euclidean distance indicates a larger discernibility of the two vectors. Specifically, the error probability to judge between two environmental conditions is dependent on the Euclidean distance between their corresponding feature vectors, which can be calculated based on Proposition 2.

**Proposition 2:** Assume that the maximum likelihood criterion is adopted to judge between  $\mathbf{c}_l$ ,  $\mathbf{c}_{l'}$  based on their corresponding feature vectors  $\mathbf{p}_{i,m}(\mathbf{c}_l; \mathbf{d}, D_q)$  and  $\mathbf{p}_{i,m}(\mathbf{c}_{l'}; \mathbf{d}, D_q)$ . Then, the error probability to judge  $\mathbf{c}_l$  erroneously as  $\mathbf{c}_{l'}$  is in inverse relation to Euclidean distance  $\|\mathbf{p}_{i,m}(\mathbf{c}_l; \mathbf{d}, D_q) - \mathbf{p}_{i,m}(\mathbf{c}_{l'}; \mathbf{d}, D_q)\|_2$  and can be calculated by

$$\text{Pr}^{\text{err}}(\mathbf{c}_{l'} | \mathbf{c}_l) = \frac{1}{2} - \frac{1}{2} \cdot \text{erf}\left(\frac{\|\mathbf{p}_{i,m}(\mathbf{c}_l; \mathbf{d}, D_q) - \mathbf{p}_{i,m}(\mathbf{c}_{l'}; \mathbf{d}, D_q)\|_2}{2\sqrt{2\sigma_{\text{M}}^2}}\right), \quad (18)$$

where  $\text{erf}(\cdot)$  denotes the *error function* [33], and  $\sigma_{\text{M}}^2$  is the variance of the measurement noise following a normal distribution.

*Proof:* See the proof of Proposition 1 in [21]. ■

As shown in Proposition 2, the error probability to judge between two environmental conditions is dependent on the Euclidean distance between feature vectors corresponding to the two

environmental conditions as well as the variance of measurement noise, i.e.,  $\sigma_M^2$ . Nevertheless, the variance of measurement noise is hard to estimate and varies for different systems and operating conditions. Thus, for generality, we evaluate the discernibility by the Euclidean distance. Therefore, based on Proposition 2 and (11)~(17), the joint sensing and transmission optimization problem of the meta-IoT structure can be formulated as follows:

$$(P1): \max_{\mathbf{d}} \Psi(\mathbf{d}) = \frac{1}{N_C N_{AR} N_{dH} N_{MD}} \cdot \left( \sum_{l=1}^{N_C} \sum_{i=1}^{N_{AR}} \sum_{m=1}^{N_{dH}} \sum_{q=1}^{N_{MD}} \|\mathbf{p}_{i,m}(\mathbf{c}_l; \mathbf{d}, D_q) - \mathbf{p}_{i,m}(\mathbf{c}_l'; \mathbf{d}, D_q)\|_2 \right), \quad (19a)$$

$$s.t. \quad y_{j,i}^{\text{large}}(f, \mathbf{d}, \mathbf{c}, h, D_q) = \gamma(f, \mathbf{d}, \mathbf{c}_l) \tilde{g}_{i,j}(f, h, D_q), \quad (19b)$$

$$\tilde{g}_{i,j}(f, h, D_q) = \frac{g_j^{\text{Tx}}(f, \theta_{j,i}^{\text{Tx}}) e^{i\varphi_{j,i}^{\text{Tx}}(f, h, D_q)} g_i^{\text{Rx}}(f, \theta_i^{\text{Rx}})}{2\beta D_w v f + 4\pi f^2 i (D_q + D_w (n_w - 1))} \cdot \sqrt{P} \cdot D_q v^2 \cdot g_{\text{sr}}(\mathbf{x}_i^{\text{Rx}}, \mathbf{x}_j^{\text{Tx}}, f, D_q) \quad (19c)$$

$$\mathbf{d} \in \mathcal{D}_A, \quad (19d)$$

$$(12), (14), (16), (17).$$

In (P1), the physical meaning of objective function  $\Psi(\mathbf{d})$  is the average discernibility of the feature vectors under different environmental conditions in terms of their Euclidean distance. Constraint (19b) indicates that the received signals are determined by reflection coefficient of meta-IoT sensors  $\gamma(f, \mathbf{d}, \mathbf{c})$  and an equivalent channel gain denoted by  $\tilde{g}_{i,j}(f, h, D)$ , which can be calculated by (19c) based on (11) and (13). It can be observed in (19b) that  $\mathbf{d}$  influences the reflection coefficients for different environmental condition  $\mathbf{c}$ , which represents the sensitivity of meta-IoT sensors, as well as the received signals given each  $\mathbf{c}$ , which represents the transmission of RF signals. Therefore, meta-IoT structure  $\mathbf{d}$  jointly influences the sensing and transmission of meta-IoT systems.

Moreover, constraint (19d) means  $\mathbf{d}$  takes value within an available meta-IoT structure set denoted by  $\mathcal{D}_A = \{\mathbf{d} = (d_1, \dots, d_i, \dots, d_{N_T}) | d_i \in [d_{\text{lb}}, d_{\text{ub}}], d_i \in \mathbb{R}, \forall i \in [1, N_T]\}$ . Specifically,  $d_{\text{lb}}$  and  $d_{\text{ub}}$  are the lower and upper bounds of the gap widths, respectively, which are acquired by using preliminary simulation trials to ensure the resonant absorption peaks of the meta-IoT sensor within frequency range  $[f_{\text{lb}}, f_{\text{ub}}]$ .

Finally, the last row of (P1) indicates that the feature vectors of the meta-IoT system follow the channel model described by (12), (14), (16) and (17). Based on (14) and (17), the feature vectors in objective function  $\Psi(\mathbf{d})$  are composed of the received signals defined by (19b). Thus,

---

**Algorithm 1** Meta-IoT structure optimization algorithm
 

---

**Input:** Set of environmental condition vectors  $\mathcal{C}$ ,  $|\mathcal{C}| = N_C$ ; Set of frequency points  $\mathcal{F}$ ,  $|\mathcal{F}| = N_F$ ; Set of available meta-IoT structures,  $\mathcal{D}_A$ ; Set of sampled meta-IoT structures with precise reflection coefficient functions,  $\hat{\mathcal{D}}_A \subset \mathcal{D}_A$ ; Distance threshold in the terminal condition for the surrogate algorithm  $v_{\min}$ .

**Output:** Optimal meta-IoT structure  $\mathbf{d}^*$ .

- 1: Fit  $\gamma(f, \mathbf{d}, \mathbf{c})$  with  $\hat{\gamma}(f, \mathbf{d}, \mathbf{c})$  in (20) given  $\mathbf{d} \in \hat{\mathcal{D}}_A$ ,  $\mathbf{c} \in \mathcal{C}$ .
  - 2: Generate a random set of samples within  $\mathcal{D}_A$ , and denote it by  $\mathcal{S}_{\text{obj}}$ .
  - 3: Evaluate the corresponding objective values in (P1) of the samples in  $\mathcal{S}_{\text{obj}}$ .
  - 4: Construct a surrogate objective function by interpolating the samples in  $\mathcal{S}_{\text{obj}}$  with a radial basis function [34].
  - 5: Generate a new set of random samples within  $\mathcal{D}_A$ , and denote it by  $\mathcal{S}_{\text{sur}}$ .
  - 6: Evaluate elements in  $\mathcal{S}_{\text{sur}}$  by the surrogate function and select the best point to be the candidate point, which is included into  $\mathcal{S}_{\text{obj}}$ .
  - 7: If all the samples in  $\mathcal{S}_{\text{sur}}$  are within the  $v_{\min}$  distance from those in  $\mathcal{S}_{\text{obj}}$ , go to Step 8; otherwise, go to Step 4.
  - 8: **return** the element in  $\mathcal{S}_{\text{obj}}$  with the current minimum objective function value as  $\mathbf{d}^*$ .
- 

the average discernibility is under the joint influence of  $\mathbf{d}$  on sensing and transmission. Therefore, by maximizing the average discernibility with respect to  $\mathbf{d}$ , both the sensing and transmission of meta-IoT sensors are optimized.

### B. Algorithm Design

In solving (P1), the challenge lies in that the unacceptable high computational complexity to evaluate the  $\Psi(\mathbf{d})$ . This is majorly due to calculating the precise reflection coefficient function, which generally has no closed-form expression and requires highly time-consuming full-wave simulation to evaluate. To handle this challenge, we first obtain a fitted function to substitute the precise reflection coefficient function. For  $n \in [1, N_F]$ , the fitted function is based on the analytical model derived in Section III-B, which can be expressed as

$$\gamma(f_n, \mathbf{d}, \mathbf{c}) = \hat{\gamma}(f_n, \mathbf{d}, \mathbf{c}) + \xi_n(\mathbf{d}, \mathbf{c}), \quad (20)$$

where  $\xi_n(\mathbf{d}, \mathbf{c})$  is an interpolated function of  $\mathbf{d}$  used to eliminate the error between the model prediction and the precise full-wave simulation results.

By using  $\gamma(f, \mathbf{d}, \mathbf{c})$  in (P1), the original optimization problem becomes a more computationally feasible. Then, as the objective function in (P1) contains the non-convex function  $\xi_n(\mathbf{d}, \mathbf{c})$  in (20), (P1) is non-convex, which is hard to solve. To solve (P1) efficiently, we can adopt efficient

algorithms such as the pattern search algorithm [35] or the surrogate optimization algorithm as in [21], which can handle finitely bounded non-convex optimization problems and has a high probability of finding global optimum. The proposed algorithm for solving (P1) is summarized as Algorithm 1. The resulting optimal meta-IoT structure vector is denoted by  $\mathbf{d}^*$ .

## VI. UNSUPERVISED SENSING ALGORITHM DESIGN FOR META-IOT SYSTEM

In this section, we handle the sensing algorithm design in the meta-IoT system. As an example, we apply the meta-IoT system to anomaly detection and localization, which is one of the most important sensing applications in 6G [36].

We first state the anomaly detection and localization problem in designing the sensing algorithm in Section VI-A and then propose an unsupervised sensing algorithm to solve it efficiently Section VI-B.

### A. Problem Statement

The anomaly detection and localization problem is stated as follows: Given a historical time-series data set  $\mathcal{T}$  which is composed of  $N_F$ -dim feature vectors collected over time  $T$ , and assuming that no anomaly exists during the data collection, the sensing algorithm aims to achieve two goals:

- **Detecting Anomaly:** Detecting a happened environmental anomaly at certain time steps after  $T$  and interpreting the environmental anomaly severity qualitatively.
- **Locating Anomaly:** Locating the position where the environmental anomaly took place.

For a sensing algorithm to achieve the above goals, it is important that the following three challenges are handled.

- 1) As environmental conditions are indicated by the frequency responses of the meta-IoT sensors, the algorithm needs to extract effective spectrum features of the received signals.
- 2) The algorithm needs to be robust with the impact of multi-path and noises, which generally exist in wireless systems.
- 3) The sensing algorithm needs to detect and locate anomalies by learning from an unlabeled data set. This is because, the meta-IoT system is designed to collect training data in an automatic manner by itself, and no auxiliary systems are adopted to inform it of the current environmental conditions.

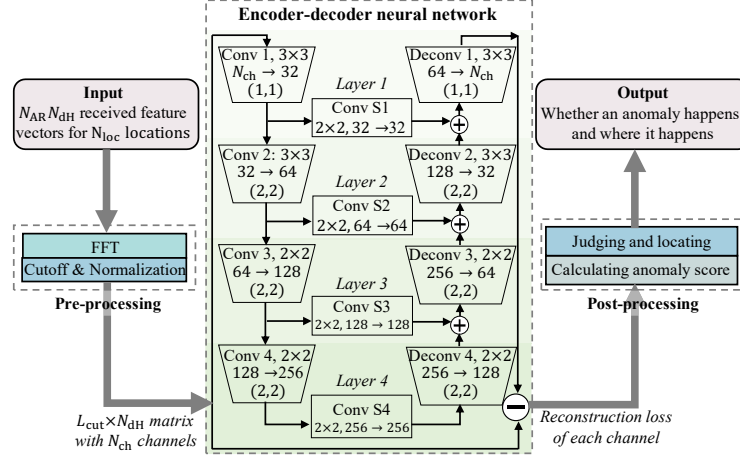


Fig. 4. Data-flow diagram of the proposed sensing algorithm.

One of the solutions is to consider the problem as a traditional channel estimation problem, where the sensing algorithm recovers the intact reflection coefficients of meta-*IoT* sensors to detect and locate anomalies. Such methods are proposed for intelligent meta-material surfaces and RFID backscatters based on deep supervised learning [37–38].

Nevertheless, in contrast to intelligent meta-material surfaces and RFID backscatters, the meta-*IoT* sensors are passive and chipless, and their reflection coefficients are determined by unknown environmental conditions. This indicates that in the meta-*IoT* systems, the sensors cannot configure themselves to predefined states and provide the training examples, e.g., pilots, which are needed in the supervised learning.

To handle the above challenges, we propose a deep unsupervised learning sensing algorithm, which is composed of a pre-processing part, a convolutional encoder-decoder neural network, and a post-processing part. Firstly, in the pre-processing part, we employ the fast Fourier transformation (FFT) to extract spectrum features from the reflected signals of each meta-*IoT* sensor array. Besides, the spectrum features obtained by FFT are further truncated, which reduces the rapid fluctuations in the spectrum features caused by multi-path and noises. Secondly, we use the convolutional encoder-decoder neural network which is efficient in noise reduction to further extract the principal information of the input features [39]. Due to the pre-processing part and the encoder-decoder neural network, the proposed sensing algorithm can also be robust

to possible external interference from other wireless systems<sup>1</sup>.

The neural network is trained by using the unsupervised learning technique with unlabeled data. In contrast to supervised learning where labeled data are in need, unsupervised learning is able to learn the similarity and differences of the measurement data within unlabeled training data set [40]. By calculating the difference between the measurement data, a sensing algorithm based on unsupervised learning can discriminate abnormal data from normal ones.

Besides, as the neural network learns directly from the collected data, it learns the relationship between the environmental conditions and the received signals automatically without relying on specific wireless propagation channels, such as dominating line-of-sight channels. Thus, though the multi-path effect makes received signals specific to wireless environments, it does not influence the environmental condition recognition of the proposed sensing algorithm. Thirdly, in the post-processing part, we compare the input and output features of the encoder-decoder neural network and derive the occurrence and location of the environmental anomalies.

### B. Algorithm Design

To solve the problem stated above, the following unsupervised sensing algorithm is proposed. The proposed algorithm takes in the feature vectors obtained from the received signals at a certain measuring distance  $D$ , and outputs indicators of the anomaly detection and localization. The complete data-flow diagram of the proposed algorithm is shown in Fig. 4, and the blocks in the diagram are introduced sequentially as follows.

**Input:** The input data to this block is the measurement data of time  $t$ . Specifically, for a measurement indexed by time  $t$ , the input data set contains the  $N_{\text{AR}}N_{\text{dH}}$  feature vectors at each location  $k$  ( $\forall k \in [1, N_{\text{loc}}]$ ), which can be expressed as

$$\mathcal{D}^t = \{\mathbf{p}_{i,m}^{k,t} \mid i \in [1, N_{\text{AR}}], m \in [1, N_{\text{dH}}], k \in [1, N_{\text{loc}}]\}. \quad (21)$$

Here,  $\mathbf{p}_{i,m}^{k,t}$  denotes the feature vector defined in (17), which is collected at time  $t$  and location  $k$  with measuring distance  $D$ , given optimal meta-IoT structure  $\mathbf{d}^*$ .

<sup>1</sup>If the extern interference is large at the frequencies of the meta-IoT sensors' resonant absorption peaks, then the performance of the sensing algorithm may decline. To handle this issue, Rx antennas with higher directionality can be used, whose main lobes are pointed at meta-IoT sensor arrays to reduce external interference.

**FFT:** In order to extract the spectrum feature from  $\mathbf{p}_{i,m}^{k,t}$ , we propose to handle the input feature vectors by using FFT. Specifically, in the *FFT* block, it applies FFT on each vector  $\mathbf{p}_{i,m}^{k,t}$  in set  $\mathcal{D}^t$ . The resulting vector of applying FFT on  $\mathbf{p}_{i,m}^{k,t}$  is denoted by  $\mathbf{P}_{i,m}^{k,t}$ .

**Cut-off & Normalization:** In this block, the results obtained by the FFT block are firstly truncated to length  $L_{\text{cut}}$ , i.e.,  $\tilde{\mathbf{P}}_{i,m}^{k,t} = ((\mathbf{P}_{i,m}^{k,t})_2, \dots, (\mathbf{P}_{i,m}^{k,t})_{L_{\text{cut}}+1})$ . Here, we remove the first element of  $\mathbf{P}_{i,m}^{k,t}$  since it indicates an average bias of the received signals, which does not contain the shape feature of the received signals' spectrum. Moreover, the *min-max normalization* is applied on the truncated vectors, which helps the training of the neural network converge faster. The min-max normalization can be expressed as

$$\hat{\mathbf{P}}_{i,m}^{k,t} = \frac{\tilde{\mathbf{P}}_{i,m}^{k,t} - \min_t(\tilde{\mathbf{P}}_{i,m}^{k,t})}{\max_t(\tilde{\mathbf{P}}_{i,m}^{k,t}) - \min_t(\tilde{\mathbf{P}}_{i,m}^{k,t})}. \quad (22)$$

Finally, for measurement time  $t$ , the normalized data is arranged as a  $N_{\text{ch}}$ -channel  $L_{\text{cut}} \times N_{\text{dH}}$  matrix, which is denoted by  $\mathcal{M}^t$ . Here,  $N_{\text{ch}} = N_{\text{AR}}N_{\text{loc}}$  denotes the number of channels. Specifically, the matrix in the  $g_{k,i}$ -th ( $g_{k,i} = (k-1) \cdot N_{\text{AR}} + i$ ,  $k \in [1, N_{\text{loc}}]$ ,  $i \in [1, N_{\text{AR}}]$ ) channel can be expressed as  $\mathbf{M}_{k,i}^t = (\hat{\mathbf{P}}_{i,1}^{k,t}, \dots, \hat{\mathbf{P}}_{i,N_{\text{dH}}}^{k,t})$ .

**Encoder-decoder Neural Network:** Data  $\mathcal{M}^t$  is passed to the encoder-decoder neural network. The encoder-decoder neural network is composed of multiple connected encoder-decoder layers, the number of which is referred to as the *depth* of the encoder-decoder neural network. To facilitate description, we describe an encoder-decoder neural network with depth 4 as used in [41], which is shown in Fig. 4 and used in the implemented prototype. The network takes  $\mathcal{M}^t$  as an input, and outputs a *difference matrix* between  $\mathcal{M}^t$  and a reconstructed  $\mathcal{M}^t$  after being encoded and decoded, which is denoted by  $\tilde{\mathcal{M}}^t$ .

Specifically, the encoder-decoder layers are composed of convolutional neural networks, which can extract feature maps as the output from input data efficiently [32]. As shown in Fig. 4, the four encoder convolutional layers are denoted by Conv 1-Conv 4, whose kernel sizes, input channel sizes, and output channel sizes are given<sup>2</sup>. For example, Conv 1 has a kernel size of  $3 \times 3$ , a stride size of  $(1, 1)$ , an input channel size  $N_{\text{ch}} = N_{\text{AR}}N_{\text{loc}}$ , and an output channel size of 32. The results of four convolutional layers are input to four *state convolutional layers*,

<sup>2</sup>The hyperparameters, including the depth of encoder-decoder neural networks, the kernel sizes, and input channel sizes, are selected following those in [41], which perform effectively in our experimental evaluations. To further optimize these hyperparameters, existing methods introduced in [42] can be used.

i.e., Conv S1~S4, whose output sizes equal to their input sizes. The four state convolutional layers provide additional capabilities for extracting the state information from feature maps at different levels.

The outputs of four state convolutional layers contain the spectrum features of the received signals at different measuring heights and the mutual dependence information of different measurement locations in different depths of encoding. Combining the outputs of the four state convolutional layers, four de-convolutional layers are used to reconstruct the original input, i.e.,  $\mathcal{M}^t$ , which are denoted by Deconv 1-Deconv 4 in Fig. 4. Each decoder layer incorporates the output of a lower decoder layer and the output of a state convolutional layer, and collectively they output the reconstruction of  $\mathcal{M}^t$ , i.e.,  $\tilde{\mathcal{M}}^t$ . By using this specific structure, the encoder-decoder neural network is effective to infer the substantial information and correlation contained in the input data and can generate accurate reconstructions while suppressing the influence of noises.

Moreover, the reconstruction loss is calculated by differencing  $\mathcal{M}^t$  and  $\tilde{\mathcal{M}}^t$ . Specifically, for the  $g_{k,i}$ -th channel, the reconstruction loss is calculated by

$$\mathcal{L}_{k,i} = \|\mathbf{M}_{k,i}^t - \tilde{\mathbf{M}}_{k,i}^t\|_2^2, \quad (23)$$

where  $\|\cdot\|_2$  indicates the  $l_2$ -norm. Then, the *mean reconstruction loss* can be defined by

$$\mathcal{L}_{\text{mean}} = \frac{1}{N_{\text{dH}}N_{\text{AR}}L_{\text{cut}}N_{\text{loc}}} \sum_{k=1}^{N_{\text{loc}}} \sum_{i=1}^{N_{\text{AR}}} \mathcal{L}_{k,i}. \quad (24)$$

Using a collected data set  $\{\mathcal{M}^t\}_t$ , we train the encoder-decoder neural network to minimize the mean reconstruction loss by using the *Adam optimization algorithm*, which is an efficient algorithm for training neural networks [32]. The training is unsupervised, where no label is provided for the data. Intuitively, when the trained encoder-decoder neural network is input with new data collected under normal conditions, it has low reconstruction loss of each channel, since the input data is essentially the same as those in the training data set except for some random noises. On the other hand, when an anomaly happens, the new data is essentially different from those in the training data set, which leads to large reconstruction losses.

**Calculating Anomaly Score:** The reconstruction loss of each channel is input into this block. As described in the previous block, the reconstruction losses can be considered as indicators for anomalies. Therefore, based on  $\mathcal{L}_{k,i}$  in (23), we propose to evaluate the anomalous degree of



the environmental conditions surrounding the  $i$ -th meta-IoT sensor array at the  $k$ -th location by using an *anomaly score* calculated by

$$\tau_{k,i}^t = \mathcal{L}_{k,i}^t / \bar{\mathcal{L}}_{k,i}. \quad (25)$$

Here,  $\bar{\mathcal{L}}_{k,i}$  denotes the average reconstruction loss of the  $g_{k,i}$ -th channel given data collected before time  $T$ , which are stored in the wireless transceiver.

**Judging and Locating:** The anomaly scores are sent to the *judging and locating* block, and the *detection indicator* of an anomaly is calculated by

$$I_{\text{ano}}^t = \begin{cases} 1, & \text{if } \Gamma = \frac{\sum_{k=1}^{N_{\text{loc}}} \sum_{i=1}^{N_{\text{AR}}} \tau_{k,i}^t}{N_{\text{loc}} N_{\text{AR}}} > \Gamma_{\text{th}}, \\ 0, & \text{otherwise.} \end{cases} \quad (26)$$

Here,  $\Gamma_{\text{th}}$  is the threshold for anomaly detection, which is selected based on average  $\Gamma$  value before  $T$ .

Given an anomaly is detected, the location of the anomaly is determined as follows. In this paper, we assume that only one anomaly may occur at a time, and the vertical and horizontal locations of the anomaly can be obtained by

$$I_{\text{ver}}^t = \operatorname{argmax}_{i \in [1, N_{\text{AR}}]} \sum_{k=1}^{N_{\text{loc}}} \tau_{k,i}^t, \quad I_{\text{hor}}^t = \operatorname{argmax}_{k \in [1, N_{\text{loc}}]} \tau_{k, I_{\text{ver}}^t}^t. \quad (27)$$

In (27),  $I_{\text{ver}}^t$  denotes the vertical location, i.e., height, of the detected anomaly, which is indicated by the index of meta-IoT sensor array. Besides,  $I_{\text{hor}}^t$  denotes the horizontal location of the detected anomaly, which is indicated by the index of measurement location.

**Output:** When  $t \leq T$ , the sensing algorithm uses data  $\mathcal{D}^t$  for training the encoder-decoder neural network to minimize  $\mathcal{L}_{\text{mean}}$ . On the other hand, when  $t > T$ , the sensing algorithm outputs detection indicator  $I_{\text{ano}}^t$  and anomaly location indicators  $(I_{\text{ver}}^t, I_{\text{hor}}^t)$  as the sensing results.

**Computational complexity analysis:** In the pre-processing part, based on the computational complexity of FFT for a vector with length  $n$  being  $\mathcal{O}(n \log_2(n))$ , the FFT calculation for all the  $N_{\text{AR}} N_{\text{loc}} N_{\text{dH}}$  feature vectors in  $\mathcal{D}^t$  is  $\mathcal{O}(N_{\text{AR}} N_{\text{loc}} N_{\text{dH}} N_F \log_2(N_F))$ . Then, the cutoff and normalization for the  $N_{\text{AR}} N_{\text{loc}} N_{\text{dH}}$  vectors have the complexity of  $\mathcal{O}(N_{\text{AR}} N_{\text{loc}} N_{\text{dH}} L_{\text{cut}})$ . Since  $L_{\text{cut}} < N_F$ , the preprocessing part has computational complexity  $\mathcal{O}(N_{\text{AR}} N_{\text{loc}} N_{\text{dH}} N_F \log_2(N_F))$ .

The encoder-decoder neural network part is composed of multiple convolutional and deconvolutional layers. Based on [43] and [44], the computational complexity of a convolutional/deconvolutional layer given a fixed kernel size can be calculated by  $\mathcal{O}(n_{\text{in}} \cdot n_{\text{out}} \cdot m_1 \cdot m_2)$

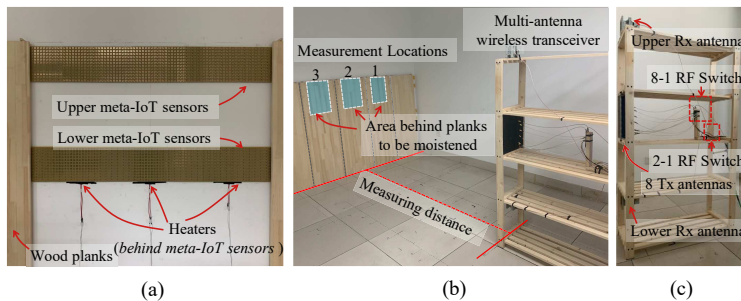


Fig. 5. Prototype implementation of the meta-IoT system. (a) Two arrays of designed meta-IoT sensors embedded behind wood planks. (b) The measurement settings deployed in a typical indoor environment, where the meta-IoT sensors are covered by the wood planks, and the multi-antenna wireless transceiver is placed at the second measurement location. (c) The multi-antenna wireless transceiver, which is installed on a wood frame.

where  $n_{\text{in}}$  and  $n_{\text{out}}$  denote the numbers of channels of the input and output data, and  $m_1$  and  $m_2$  denote the side-lengths of output data. Thus, based on the network structure information shown in Fig. 4, the computational complexity of the encoder-decoder neural network part is dominated by those of the Conv 1 and Deconv 1, which are both  $\mathcal{O}(L_{\text{cut}}^2 N_{\text{dH}}^2 N_{\text{ch}})$ .

Finally, in the post-processing part, based on (25)~(27), the computational complexity is  $\mathcal{O}(N_{\text{ch}})$ . Therefore, in summary, the computational complexity of the sensing algorithm is dominated by those of the preprocessing and encoder-decoder neural network parts, which can be expressed by  $\mathcal{O}(N_{\text{AR}} N_{\text{loc}} N_{\text{dH}} N_F \log_2(N_F) + L_{\text{cut}}^2 N_{\text{dH}}^2 N_{\text{ch}})$ .

**Remark:** In Section IV-A, we assume that the meta-IoT sensors are embedded at depth  $D_w \geq 0$ . As the received signal model proposed in Section IV-B and the designed algorithms in Section V and this section are not dependent on the specific value of  $D_w$ , the proposed method is suitable for both  $D_w > 0$  and  $D_w = 0$  cases, i.e., the embedded and non-embedded scenarios.

## VII. IMPLEMENTATION

In this section, we elaborate on the implementation of the meta-IoT system. The prototype system is tested in a typical indoor environment and is applied to detecting and locating temperature and humidity anomalies inside walls. The detailed information of the meta-IoT sensors and the multi-antenna wireless transceiver is provided in Sections VII-A and VII-B, respectively.

### A. Meta-IoT Sensors

Based on the optimal meta-IoT structure design obtained in Section V, we fabricate the meta-IoT sensors. Each meta-IoT sensor contains  $N_T = 2$  meta-IoT sensor units, and each meta-IoT

sensor unit has a size of  $l_s \times l_s \times h_s = 14.54 \times 14.54 \times 3.2 \text{ mm}^3$ . The SRRs of the two meta-IoT sensor units are made of copper lines with  $W_{\text{SRR}} = 1.2 \text{ mm}$  width and  $H_{\text{SRR}} = 0.035 \text{ mm}$  thickness. Besides, the side length of the SRRs is  $L_{\text{SRR}} = 7.5 \text{ mm}$ , and the gap widths of the two SRRs are  $d^* = (1.126, 1.761) \text{ mm}$ , respectively, which are obtained by solving (P1). In a meta-IoT sensor, the first meta-IoT sensor unit has humidity-sensitive materials filled in its gap, which are the polymer used in the hygistor TELAiRE HS30P [45]. The second meta-IoT sensor unit has temperature-sensitive materials within its gap, which we are the power of thermistor SDNT2012X102-3450-TF [46]. Moreover, the substrate of each meta-IoT sensor unit is FR-4, and the bottom is covered with a thin copper plane to enhance reflection.

As shown in Fig. 5 (a), the meta-IoT sensors are arranged into two rectangle arrays, i.e., an upper meta-IoT sensor array and a lower meta-IoT sensor array, which are pasted onto a vertical surface. The upper and lower meta-IoT sensor arrays are installed at  $h_1^{\text{MS}} = 110 \text{ cm}$  and  $h_2^{\text{MS}} = 58 \text{ cm}$ , respectively, and have a horizontal length of  $191.4 \text{ cm}$  and a vertical width of  $L_{\text{MS}} = 17.4 \text{ cm}$ . Each meta-IoT sensor array contains 792 meta-IoT sensors.

To imitate the scenario where the meta-IoT sensor arrays are embedded inside the wall, we adopt wood planks to cover the meta-IoT sensor arrays. This setup is based on the experimental observations in [47]: for signals within  $2.4 \sim 5 \text{ GHz}$ , wooden walls have a similar attenuation effect with concrete walls. Besides, according to the standard for engineering acceptance of generic cabling systems [48], the cables buried inside a wall should be at least  $30 \text{ mm}$  in depth. Therefore, we use 5 wood planks with a thickness of  $30 \text{ mm}$  to cover the meta-IoT sensor arrays, each of which has a size of  $120 \times 40 \text{ cm}^2$ . The complete setup is shown in Fig. 5 (b), where  $N_{\text{loc}} = 3$  measurement locations are considered.

For each measurement location, we consider two types of anomalies, i.e., humidity anomalies and temperature anomalies. Based on [49], we imitate the humidity anomalies inside walls by adding a moistened layer in the upper backside region of a wood plank, which is illustrated in Fig. 5 (b). Specifically, the moistened layer is composed of a piece of wet thin paper, which itself has neglectable influence on the wireless signals. The vertical length of the moistened layer is  $40 \text{ cm}$ , and the horizontal width of the moistened layer is denoted by  $W_{\text{M}} = 17.5 \text{ cm}$ .

Besides, as in [50], we control the environmental temperature by using heaters, which are installed behind the lower meta-IoT sensor array at each measurement location to generate temperature anomalies. Given heating power  $P_{\text{heat}} = 40 \text{ W}$ , each heater is able to heat the adjacent meta-IoT sensors to be higher than  $40^\circ\text{C}$  when the wall temperature is  $18^\circ\text{C}$ . Therefore,

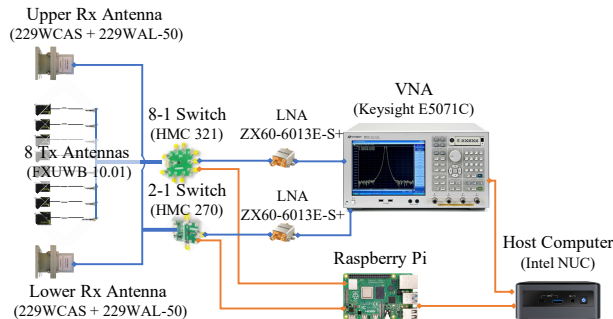


Fig. 6. Hardware schematic of the implemented multi-antenna wireless transceiver. Blue lines indicate the RF signal links, and the yellow lines indicate the baseband links for data and control signals.

the temperature difference between the normal and anomalous conditions is larger than  $22^{\circ}\text{C}$ , which satisfies the standard for testing anomalous conditions of electrical equipments (i.e., to be larger than  $16^{\circ}\text{C}$ ) as required by National Fire Protection Association (NFPA) [51].

### B. Multi-antenna Wireless Transceiver

Fig. 5 (c) shows the implemented multi-antenna wireless transceiver. Besides, its detailed hardware components are shown in Fig. 6 and described as follows.

1) *Tx Antenna Array*: The Tx antenna array contains  $N_{\text{AT}} = 8$  Tx antennas, for which we adopt the Taoglas FXUWB10.01 linearly-polarized patch antenna. The spacing interval between adjacent Tx antennas is  $\delta^{\text{AT}} = 3.67$  cm. Besides, the center of the Tx array is at a height of  $h_c^{\text{AT}} = 83.6$  cm and is aligned with the center line of the measurement location. Moreover, a piece of wave-absorbing material is placed behind the Tx antennas. This setting makes the Tx antennas directional, which satisfies the requirement for the wireless transceiver in Section IV.

2) *Rx Antennas*: We adopt  $N_{\text{AR}} = 2$  waveguide Rx antennas, each of which is composed of a waveguide-to-coax adapter (229WCAS) and a rectangular waveguide (229WAL-50). The upper and lower Rx antennas are at heights of  $h_1^{\text{AR}} = 136.3$  cm and  $h_2^{\text{AR}} = 32$  cm, respectively.

3) *Radio-frequency (RF) Switches*: To reduce the number of RF chains needed in the wireless transceiver, we adopt two RF switches to multiplex single Tx and Rx chains. Specifically, the 8 Tx antennas are connected to a single-pole-8-throw RF switch (HMC 321), and the 2 Rx antennas are connected to a single-pole-2-throw RF switch (HMC 270).

4) *Low Noise Amplifiers (LNA)*: The poles of the two RF switches are connected to the ports of two LNAs (ZX-60-43-S+), which are able to provide an average gain of about 13.5 dB

TABLE I  
SYSTEM PARAMETERS

Parameter	Value	Parameter	Value
Number of Rx antennas ( $N_{AR}$ )	2	Center heights of meta-IoT sensor arrays ( $h_1^{MS}, h_2^{MS}$ )	110, 58 cm
Number of Tx antennas ( $N_{AT}$ )	8	Center height of Tx antenna array ( $h_c^{AT}$ )	83.6 cm
Frequency band of signals ( $[f_{lb}, f_{ub}]$ )	[3.5, 4] GHz	Space interval between adjacent Tx antennas ( $\delta^{AT}$ )	3.67 cm
Number of sensing targets/meta-IoT units ( $N_T$ )	2	Heights of Rx antennas ( $h_1^{AR}, h_2^{AR}$ )	(136.3, 32) cm
Side length of meta-IoT sensor unit ( $l_s$ )	14.54 mm	Default measuring distance ( $D$ )	1 m
Side length of SRR ( $L_{SRR}$ )	7.5 mm	Number of measurement locations ( $N_{loc}$ )	3
Width of SRR ( $W_{SRR}$ )	1.2 mm	Vertical width of a meta-IoT sensor array ( $L_{MS}$ )	17.4 cm
Thickness of SRR ( $H_{SRR}$ )	0.035 mm	Transmit power ( $P_T$ )	10 dBm
Gap widths of meta-IoT sensor units ( $d^*$ )	(1.126, 1.761) mm	Number of height displacement ( $N_{dH}$ )	60
Number of frequency points ( $N_F$ )	501	Truncation length for FFT results ( $L_{cut}$ )	60
Standard deviation of measuring noise ( $\sigma_M$ )	$10^{-3}$	Default width of moistened area ( $W_M$ )	17.5 cm
Distance threshold in Algorithm 1 ( $v_{min}$ )	$10^{-3}$	Default heating power ( $P_{heat}$ )	40 W

at [3.5, 4] GHz. The LNAs are able to amplify the transmitted signals sent to the Tx antennas as well as the received signals from the Rx antennas.

5) *Vector Network Analyzer (VNA)*: We use a two-port VNA (Keysight E50171C) as the signal transceiver. Specifically, the VAN is set to the forward transmission coefficient, i.e.,  $S_{21}$  measurement mode, in order to measure the reflected signals from the meta-IoT sensors.

6) *Raspberry Pi*: We adopt a Raspberry Pi to control the RF switches selecting which Tx antenna and Rx antenna are connected to the ports of the VNA.

7) *Host Computer*: The host computer serves as the core controller and data processor of the multi-antenna wireless transceiver. Through Ethernet, it sends control signals to the VNA and the Raspberry Pi and receives the  $S_{21}$  measurement results from the VNA. Besides, the sensing algorithm in Section VI-B is implemented in the host computer by Python.

## VIII. EVALUATION

In this section, we evaluate the effectiveness of the proposed meta-IoT system. Specifically, we first provide simulation results for the optimal meta-IoT structure obtained by Algorithm 1. Then, we provide the experimental results for the multi-antenna wireless transceiver to validate its capability of sensing meta-IoT sensor arrays at different heights. Following that, we provide the experimental results for the prototype system to detect and locate humidity and temperature anomalies, in the cases of different measuring distances, anomaly scales, noise levels, and depths of the neural network. The detailed parameters of the system are summarized in Table I.

Firstly, to evaluate the effectiveness of the proposed analytical reflection coefficient model in Section III-B, we compare its computation time with that of the full-wave simulation in the

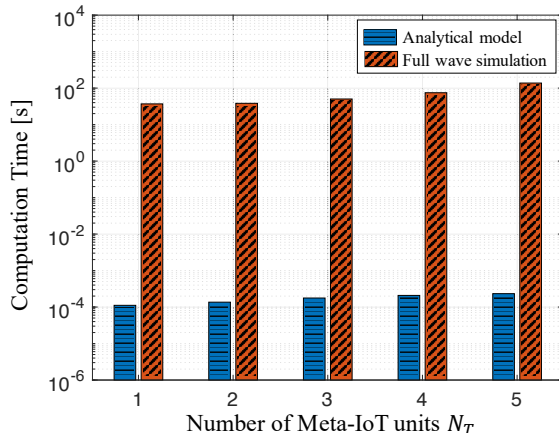


Fig. 7. Comparison between computation time of reflection coefficient using analytical model and full wave simulation.

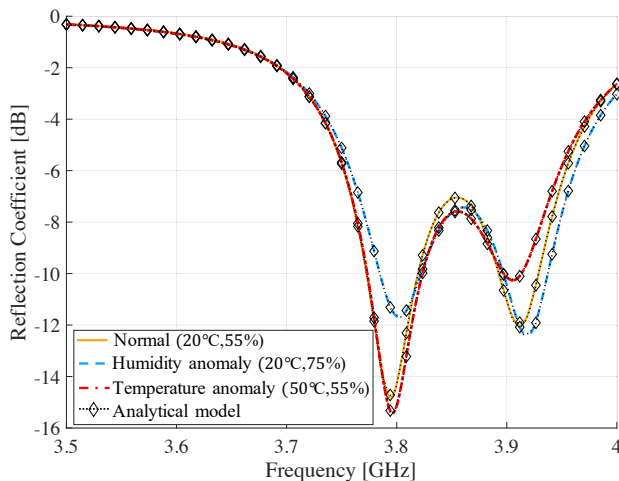


Fig. 8. Reflection coefficients of meta-IoT sensor given  $d^*$ , in the cases of normal, humidity anomaly, and temperature anomaly environmental conditions. The solid and dash lines indicate the results of the full-wave simulation, and the dotted lines with diamond marks indicate the results of the analytical model.

CST software. As shown in Fig. 7, it can be observed that the computation time of calculating the reflection coefficient using the analytical model is around 5 orders of magnitude lower than that of the full-wave simulation.

Then, the evaluation of the optimal meta-IoT structure obtained by Algorithm 1 is provided. Specifically, when solving Algorithm 1, the same system parameters used in the experimental evaluation in Table I are adopted. Besides, the additional parameters in the simulation can be explained as follows. The thickness of the wall  $D_w = 30$  mm, and the relative index of refraction of the wall is  $n_w = 4.2$  based on [47]. Moreover, we consider the performance of meta-IoT

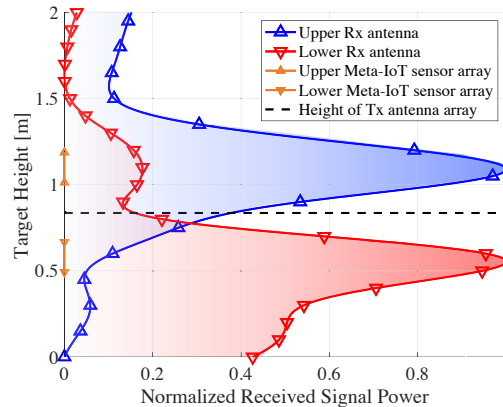


Fig. 9. Normalized received signal power obtained by the upper and lower Rx antennas when the Tx antenna array applies digital beamforming to steer its beam to different target heights. The received signal power of each antenna is re-scaled through min-max normalization to facilitate observation.

sensors in three environmental condition cases, which are the normal case (temperature  $20^{\circ}\text{C}$ , humidity  $55\%$ ), temperature anomaly case (temperature  $50^{\circ}\text{C}$ , humidity  $55\%$ ), and humidity anomaly case (temperature  $20^{\circ}\text{C}$ , humidity  $75\%$ ). Based on [45–46], the conductivities of the temperature sensitive material in normal and anomaly cases are  $0.32$  and  $0.97$  [S/m], and those of the humidity sensitive material are  $0.11$  and  $0.67$  [S/m], respectively. Furthermore, the available meta-IoT structure set is  $\mathcal{D}_A = \{\mathbf{d} | d_i \in [0.5, 2], d_i \in \mathbb{R}, i = 1, 2\}$ , which ensures the resonant absorption peaks of the two SRRs within  $[3.5, 4]$  GHz, and the sampled meta-IoT structure set is  $\hat{\mathcal{D}}_A = \{\mathbf{d} | d_i \in \{0.5, 1, 1.5, 2\}, i = 1, 2\}$ . Given the above simulation setting, the optimal meta-IoT structure obtained by Algorithm 1 is  $\mathbf{d}^* = (1.126, 1.761)$  mm.

In Fig. 8, it can be observed that given  $\mathbf{d}^*$ , there exist two distinct reflection coefficient valleys, which are due to the resonance absorption of first and second meta-IoT units, respectively. Moreover, when a humidity/temperature anomaly happens, the reflection coefficients at the frequencies around the first/second valley become significantly larger, which can be measured by the wireless transceiver. This lays the foundation for the proposed system to detect humidity and temperature anomalies. Furthermore, the results of the analytical reflection coefficient model in (20) are in accordance with the results of the full-wave simulation in different cases, which verifies the effectiveness of the analytical model.

Fig. 9 shows the normalized received signal power obtained by the upper and lower Rx antennas when the digital beamforming is used to extract reflected signals by the meta-IoT sensors at different heights. It can be observed that when the target height falls into the height

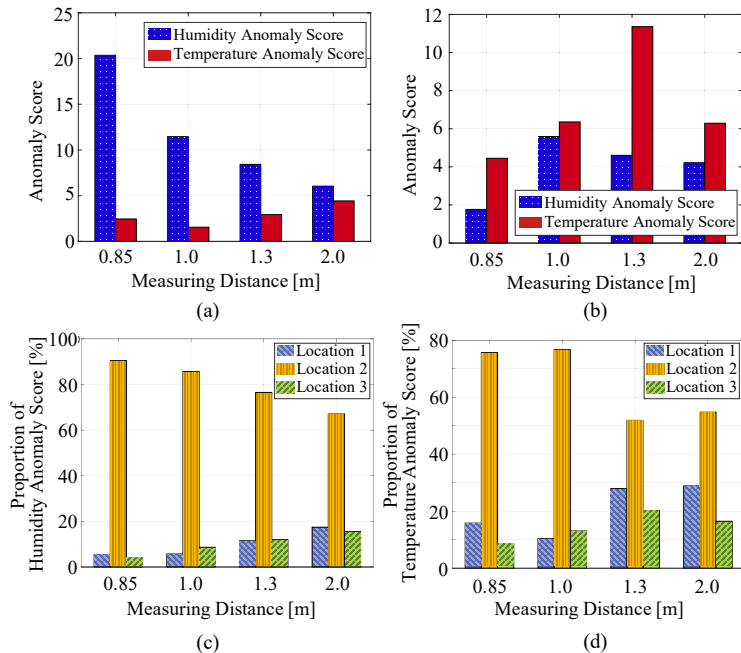


Fig. 10. Anomaly scores when (a) a humidity anomaly or (b) a temperature anomaly happens at Location 2, under different measuring distances. Besides, (c) and (d) show the proportions of anomaly scores corresponding to different locations under different measuring distances, when the humidity and temperature anomalies happen, respectively.

ranges of the upper and lower meta-IoT sensor arrays, the received signal power reaches its maximum. This verifies that the designed algorithm can suppress multi-path effects so that the reflected signals by meta-IoT sensor arrays at different heights can be obtained separately. Besides, Fig. 9 also verifies that by setting the added phases according to (16), the arriving phases of the signals which travel from different Tx antennas to the Rx antennas via the meta-IoT sensors at the target height are successfully aligned. Since the added phases are determined based on the received signal model, Fig. 9 also provides experiential verification for the received signal model in (11) proposed in Section IV-B.

In Figs. 10 (a) and (b), it can be observed that within the measuring distance range from 0.85 m to 2 m, the accurate anomaly type can be obtained by (27), which also indicates that the vertical locations of the anomalies are obtained correctly. Specifically, when a humidity/temperature anomaly occurs, the humidity/temperature anomaly scores at different measuring distances are larger than the temperature/humidity anomaly scores. Moreover, from Figs. 10 (c) and (d), it can be seen that within the range from 0.85 m to 2 m, the accurate horizontal location of the happened anomaly, i.e., Location 2, can be obtained correctly.



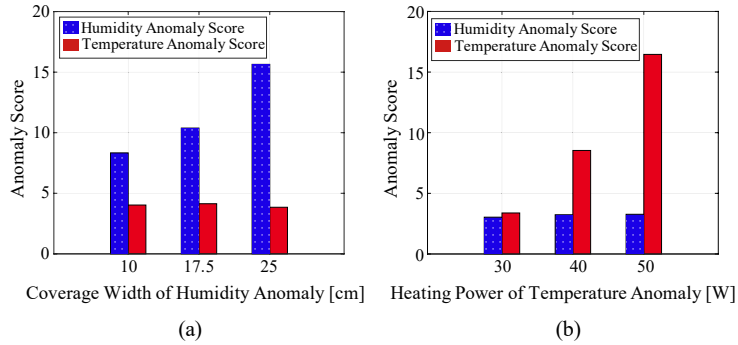


Fig. 11. Humidity and temperature anomaly scores for (a) a humidity anomaly with different coverage widths, and (b) for a temperature anomaly with different heating power.

Furthermore, a larger difference between the anomaly scores indicates a higher capability of the prototype system to detect and locate the anomaly. In Figs. 10 (a) and (c), the difference between the humidity and temperature anomaly scores and the difference between the proportion of humidity anomaly score of Location 2 and those of the other locations become smaller as measuring distance increases. This indicates that the capability of the prototype in terms of anomaly detection and localization decreases with the measuring distance, which is due to that the received signal power decreases with the measuring distance. Nevertheless, in Figs. 10 (b) and (d), the capability of the prototype to detect and locate a temperature anomaly is not monotonically decreasing with the measuring distance. This is because the propagation of the signals reflected by the lower meta-IoT sensor array follows a *two-ray* model due to the floor reflection, and thus the received signal power is not in a monotone relationship with the measuring distance.

Figs. 11 (a) and (b) show the humidity and temperature anomaly scores for a humidity anomaly with different coverage widths of the moistened layer, and for a temperature anomaly with different heating power, respectively. It can be seen that given a humidity anomaly or a temperature anomaly with different degrees, the proposed system can judge the type, i.e., the vertical location, of the anomaly correctly. Besides, with the increment of the coverage width of the humidity anomaly and the heating power of the temperature anomaly, the humidity and temperature anomaly scores increase, respectively. Therefore, by comparing the relative anomaly scores, the proposed system can potentially estimate the degree of anomaly.

In Fig. 12, the false alarm ratio decreases with the miss detection ratio, which can be obtained by increasing the threshold for anomaly detection in (26). Therefore, there exists a tradeoff in selecting the threshold for anomaly detection. Moreover, with the increment of SNR

TABLE II  
COMPARISON OF THE PROPOSED SYSTEM WITH EXISTING WORKS

Parameters	Sensing Target	Frequency Band	Experimental Environment	LoS Existence	Deployment Scale	Sensitivity	Transmission Range	Require Labeled Data
<b>Proposed</b>	Humidity and temperature anomalies	3.5-4.0 GHz	Indoor office	No	Multiple sensor arrays	1.64%/°C, 5.25%/%	2 m	No
[13]	Temperature level	2.2-2.6 GHz	Air-tight box	Yes	Single sensor	1.23%/°C	0.2 m	Yes
[15]	Humidity level	6.5-9.0 GHz	Air-tight box	Yes	Single sensor	0.12%/%	0.3 m	Yes
[16]	Humidity level	3-4 GHz	Anechoic chamber	Yes	Single sensor	0.26%/%	0.5 m	Yes
[18]	Temperature level	9-15 GHz	Sample holder box	No	Single array	0.05%/°C	0.5 m	Yes
[19]	Humidity level	2.7-3.05 GHz	Waveguide	Yes	Single sensor	2.68%/%	NA	Yes

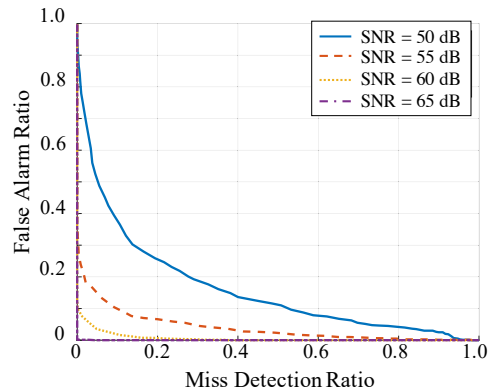


Fig. 12. False alarm ratio versus miss detection ratio of the proposed system under different SNR levels of the received signals.

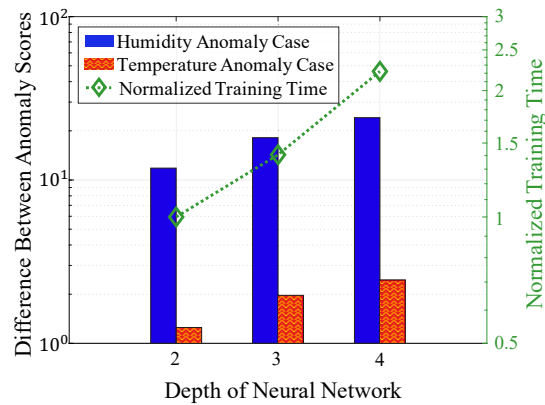


Fig. 13. Difference between anomaly scores and normalized training time versus depth of the encoder-decoder neural network in different anomaly cases, where the minimal training time is normalized to 1.

of the received signals, both the false alarm ratio and the miss detection ratio can be reduced. Furthermore, when  $\text{SNR} \geq 65$  dB, the proposed system is able to detect an anomaly accurately.

In Fig. 13, as the depth of the encoder-decoder neural network increases, the difference between anomaly scores and the normalized training time have approximately exponential growth. Nevertheless, the slope of the training time increment is higher than that of the difference between anomaly scores. Therefore, using an encoder-decoder neural network with a depth larger than 4 will result in a significant increment of the training time. This verifies the 4-leveled encoder-decoder neural network used in the sensing algorithm as it can detect and locate an anomaly accurately without requiring a large amount of training time.

As a summary, we compare the proposed system with the existing works mentioned in Section II which use passive chipless sensors working in a similar frequency band and having similar functions. The comparison results are shown in Table II, where the *sensitivity* is defined by the deviation of the minimum reflected coefficient for a unit environmental condition change, i.e., for 1°C temperature or 1% humidity. From Table II, the following three conclusions can be made.

Firstly, compared with the existing works, the proposed system has higher sensitivities with respect to the humidity and temperature conditions, and achieves a longer transmission range. This is because the size of a meta-IoT sensor unit being smaller than half of the working wavelength enables a larger number of meta-IoT sensor units to be filled into a given area. Besides, it makes the reflected signal power of a meta-IoT sensor array more concentrated, according to the antenna array theory [17]. Secondly, the deployment scale of the proposed system is the largest compared with the existing works, where multiple arrays of sensors are installed to detect and locate anomalies within a large region. Therefore, the proposed system is more suitable for 6G, which requires the sensors to be densely deployed on a large scale. Thirdly, the proposed system does not rely on labeled data, since its sensing algorithm is trained in an unsupervised manner. Thus, the proposed system especially fits for the applications of anomaly detection and localization, since the anomalous data are generally unavailable in advance.

## IX. CONCLUSION

In this paper, we have considered a meta-IoT system with a large number of meta-IoT sensors, and have proposed a joint sensing and transmission design for this system. Specifically, we have first modeled the signal at the receiver considering the joint influence of sensing and transmission. Based on this model, we have optimized the meta-IoT sensor design for the sensing performance.

Then, we have designed an unsupervised sensing algorithm based on a convolutional encoder-decoder neural network, which can robustly sense environmental anomalies.

Based on the experimental evaluations of the prototype, we can offer the following conclusions.

- Firstly, compared with other existing works, the designed system has a higher sensitivity and a longer transmission range. The prototype system has demonstrated the capability to successfully detect and locate anomalies within 2 m and distinguish the locations of anomalies with a spatial resolution of 0.4 m.
- Secondly, by using the designed sensing algorithm, multi-path effects can be suppressed so that the signals reflected by different meta-IoT sensor arrays can be obtained separately.
- Thirdly, the proposed system has been shown to be robust to noises. To be specific, the false alarm and miss detection ratios of the prototype system decrease with the SNR, and approach zero for SNRs larger than 65 dB, given the typical indoor environment.

## APPENDIX A

### PROOF OF PROPOSITION 1

Since a larger number of meta-IoT sensors can be collectively considered as a uniform effective medium, the meta-IoT sensor array performs specular reflection according to the principles of geometric optics. The equivalent reflection coefficient is denoted by  $\chi(f, \mathbf{d}, \mathbf{c}, D)$ . Thus, (11) can be derived. Moreover,  $\chi(f, \mathbf{d}, \mathbf{c}, D)$  can be calculated by the following special case. For an infinite meta-IoT sensor array surface, consider that a Tx antenna and a Rx antenna which are superimposed and both at distance  $D$  from the meta-IoT sensor array. Then, based on general channel model (5), the received signal at the Rx antenna can be calculated by

$$\begin{aligned} y(f, \mathbf{d}, \mathbf{c}, D) &= \sqrt{P} \cdot g^{\text{Tx}}(f) \cdot g^{\text{Rx}}(f) \cdot \gamma(f, \mathbf{d}, \mathbf{c}) \cdot \iint_{-\infty}^{\infty} \left( \frac{v e^{-\sqrt{D^2+y^2+z^2}(\beta \frac{D_w}{D} + i(\frac{2\pi f}{v} + \frac{2\pi f D_w}{v D}(n_w-1)))}}{4\pi f \sqrt{D^2+y^2+z^2}} \right)^2 yz \\ &= \sqrt{P} \cdot g^{\text{Tx}}(f) \cdot g^{\text{Rx}}(f) \cdot \gamma(f, \mathbf{d}, \mathbf{c}) \cdot \frac{v^2}{16\pi^2 f^2} \cdot 2\pi \cdot \text{Ei}\left(2D \cdot \left(\beta \frac{D_w}{D} + i\left(\frac{2\pi f}{v} + \frac{2\pi f D_w}{v D}(n_w-1)\right)\right)\right) \end{aligned} \quad (28)$$

where  $\text{Ei}(\vartheta)$  denotes the exponential integration function. Based on the property  $\text{Ei}(\vartheta) = \frac{e^{-\vartheta}}{\vartheta} \sum_{k=0}^{K-1} \frac{k!}{(-\vartheta)^k}$ , when  $D$  is large, (28) can be approximated by

$$y(f, \mathbf{d}, \mathbf{c}, D) \approx \sqrt{P} \cdot g^{\text{Tx}}(f) \cdot g^{\text{Rx}}(f) \cdot \underbrace{\frac{Dv^2 \gamma(f, \mathbf{d}, \mathbf{c})}{2\beta D_w v f + 4\pi f^2 i(D + D_w(n_w-1))}}_{\text{Coefficient } \chi(f, \mathbf{d}, \mathbf{c}, D)} \cdot \underbrace{\frac{v e^{-(\beta \frac{D_w}{D} + i(\frac{2\pi f}{v} + \frac{2\pi f D_w}{v D}(n_w-1))) \cdot 2D}}{4\pi f \cdot 2D}}_{\text{Specular Reflection } g_{\text{sr}}(\mathbf{x}^{\text{Rx}}, \mathbf{x}^{\text{Tx}}, f, D)},$$

which proves (13) in Proposition 1. ■

## REFERENCES

- [1] M. F. Othman and K. Shazali, "Wireless sensor network applications: A study in environment monitoring system," *Procedia Eng.*, vol. 41, pp. 1204–1210, Aug. 2012.
- [2] S. Zhang, H. Zhang, and L. Song, "Beyond D2D: Full dimension UAV-to-everything communications in 6G," *IEEE Trans. Veh. Technol.*, vol. 69, no. 6, pp. 6592–6602, Jun. 2020.
- [3] G. Wikström, J. Peisa, P. Rugeland, N. Johansson, S. Parkvall, M. Girnyk, G. Mildh, and I. L. Da Silva, "Challenges and technologies for 6G," in *Proc. IEEE 6G Wireless Summit*, Levi, Finland, Mar. 2020.
- [4] T. Huang, W. Yang, J. Wu, J. Ma, X. Zhang, and D. Zhang, "A survey on green 6G network: Architecture and technologies," *IEEE Access*, vol. 7, pp. 175 758–175 768, Dec. 2019.
- [5] E. Zanj, G. Caso, L. De Nardis, A. Mohammadpour, O. Alay, and M.-G. Di Benedetto, "Energy efficiency in short and wide-area iot technologies—a survey," *Technol.*, vol. 9, no. 1, Mar. 2021.
- [6] M. Lauridsen, R. Krigslund, M. Rohr, and G. Madueno, "An empirical NB-IoT power consumption model for battery lifetime estimation," in *Proc. IEEE Veh. Technol. Conf.*, Porto, Portugal, Jun. 2018.
- [7] A. Nikoukar, S. Raza, A. Poole, M. Güneş, and B. Dezfouli, "Low-power wireless for the Internet of Things: Standards and applications," *IEEE Access*, vol. 6, no. 1, pp. 67 893–67 926, Nov. 2018.
- [8] F. Costa, S. Genovesi, M. Borgese, A. Michel, F. A. Dicandia, and G. Manara, "A review of RFID sensors, the new frontier of Internet of Things," *Sens.*, vol. 21, no. 9, p. 3138, 2021.
- [9] P. Mezzanotte, V. Palazzi, F. Alimenti, and L. Roselli, "Innovative RFID sensors for Internet of Things applications," *IEEE J Microwaves*, vol. 1, no. 1, pp. 55–65, Jan. 2021.
- [10] E. Ozturk, M. Dikkers, K. Batenburg, C. Salm, and J. Schmitz, "RFID tag failure after thermal overstress," in *IEEE Int. Integr. Reliab. Workshop*, South Lake Tahoe, CA, Oct. 2019.
- [11] J. Hu, H. Zhang, B. Di, L. Li, K. Bian, L. Song, Y. Li, Z. Han, and H. V. Poor, "Reconfigurable intelligent surface based RF sensing: Design, optimization, and implementation," *IEEE J. Sel. Areas Commun.*, vol. 38, no. 11, pp. 2700–2716, Nov. 2020.
- [12] H. Zhang, B. Di, K. Bian, Z. Han, H. V. Poor, and L. Song, "Towards ubiquitous sensing and localization with reconfigurable intelligent surfaces," *Proc. IEEE*, May 2022, early access, arXiv:2201.10101.
- [13] A. Vena, L. Sydänheimo, M. M. Tentzeris, and L. Ukkonen, "A fully inkjet-printed wireless and chipless sensor for CO<sub>2</sub> and temperature detection," *IEEE Sens. J.*, vol. 15, no. 1, pp. 89–99, Jul. 2015.
- [14] J. G. D. Hester and M. M. Tentzeris, "Inkjet-printed flexible mm-Wave van-atta reflectarrays: A solution for ultralong-range dense multitag and multisensing chipless RFID implementations for IoT smart skins," *IEEE Trans. Microw. Theory Techn.*, vol. 64, no. 12, pp. 4763–4773, Nov. 2016.
- [15] E. M. Amin, S. Bhuiyan, N. Karmakar, and B. Winther-Jensen, "A novel EM barcode for humidity sensing," in *Proc. IEEE Int. Conf. RFID*, Orlando, FL, Apr. 2013.
- [16] F. Deng, Y. He, B. Li, Y. Song, and X. Wu, "Design of a slotted chipless RFID humidity sensor tag," *Sens. Actuators B Chem.*, vol. 264, pp. 255–262, Jul. 2018.
- [17] A. Goldsmith, *Wireless Communications*. New York, NY: Cambridge University Press, 2005.

- [18] H. Karim, D. Delfin, L. A. Chavez, L. Delfin, R. Martinez, J. Avila, C. Rodriguez, R. C. Rumpf, N. Love, and Y. Lin, "Metamaterial based passive wireless temperature sensor," *Adv. Eng. Mater.*, vol. 19, no. 5, pp. 1–8, Feb. 2017.
- [19] E. Ekmekci, U. Kose, A. Cinar, O. Ertan, and Z. Ekmekci, "The use of metamaterial type double-sided resonator structures in humidity and concentration sensing applications," *Sens. Actuator A Phys.*, vol. 297, pp. 1–15, Oct. 2019.
- [20] J. Hu, H. Zhang, B. Di, K. Bian, and L. Song, "Meta-material sensors based Internet of Things for 6G communications," in *Proc. IEEE Global Commun. Conf.*, Madrid, Spain, Dec. 2021.
- [21] J. Hu, H. Zhang, B. Di, Z. Han, H. V. Poor, and L. Song, "Meta-IoT: Simultaneous sensing and transmission by meta-material sensor based Internet of Things," *IEEE Trans. Wireless. Commun.*, vol. pp, no. 99, pp. 1–1, Feb. 2022, early access.
- [22] X. Liu, J. Hu, H. Zhang, B. Di, and L. Song, "Deployment optimization for meta-material based Internet of Things," in *Proc. IEEE Global Commun. Conf.*, Madrid, Spain, Dec. 2021.
- [23] B. A. Munk, *Frequency Selective Surfaces: Theory and Design*. New York, NY: John Wiley & Sons, 2005.
- [24] D. M. Pozar, *Microwave Engineering*. New York, NY: Wiley, 2011.
- [25] W. Tang, X. Li, J. Y. Dai, S. Jin, Y. Zeng, Q. Cheng, and T. J. Cui, "Wireless communications with programmable metasurface: Transceiver design and experimental results," *China Commun.*, vol. 16, no. 5, pp. 46–61, Jun. 2019.
- [26] W. Withayachumnankul, K. Jaruwongrunsee, A. Tuantranont, C. Fumeaux, and D. Abbott, "Metamaterial-based microfluidic sensor for dielectric characterization," *Sens. Actuator A Phys.*, vol. 189, pp. 233–237, Jan. 2013.
- [27] H. Kairm, D. Delfin, M. A. I. Shuvo, L. A. Chavez, C. R. Garcia, J. H. Barton, S. M. Gaytan, M. A. Cadena, R. C. Rumpf, R. B. Wicker, Y. Lin, and A. Choudhuri, "Concept and model of a metamaterial-based passive wireless temperature sensor for harsh environment applications," *IEEE Sensors J.*, vol. 15, no. 3, pp. 1445–1452, Oct. 2015.
- [28] D. S. Jones, *The Theory of Electromagnetism*. Headington Hill Hall, Oxford: Pergamon Press LTD., 2013.
- [29] S. Zhang, H. Zhang, B. Di, and L. Song, "Cellular UAV-to-X communications: Design and optimization for multi-UAV networks," *IEEE Trans. Wireless Commun.*, vol. 18, no. 2, pp. 1346–1359, Feb. 2019.
- [30] W. Tang, M. Z. Chen, X. Chen, J. Y. Dai, Y. Han, M. Di Renzo, Y. Zeng, S. Jin, Q. Cheng, and T. J. Cui, "Wireless communications with reconfigurable intelligent surface: Path loss modeling and experimental measurement," *IEEE Trans. Wireless Commun.*, vol. 20, no. 1, pp. 421–439, Jan. 2021.
- [31] H. Lu and Y. Zeng, "Communicating with extremely large-scale array/surface: Unified modeling and performance analysis," *IEEE Trans. Wireless Commun.*, vol. 21, no. 6, pp. 4039–4053, Jan. 2022.
- [32] I. Goodfellow, Y. Bengio, and A. Courville, *Deep Learning*. Cambridge, MA: MIT Press, 2016.
- [33] R. N. McDonough and A. D. Whalen, *Detection of Signals in Noise*. San Diego, CA: Academic Press, 2004.
- [34] M. D. Buhmann, *Radial Basis Functions: Theory and Implementations*. Cambridge, UK: Cambridge

- University Press, 2004.
- [35] Y. Wang and C. A. Shoemaker, "A general stochastic algorithmic framework for minimizing expensive black box objective functions based on surrogate models and sensitivity analysis," *arXiv:1410.6271*, Oct. 2014.
- [36] G. Han, J. Tu, L. Liu, M. Martínez-García, and Y. Peng, "Anomaly detection based on multidimensional data processing for protecting vital devices in 6G-enabled massive IIoT," *IEEE Internet Things J.*, vol. 8, no. 7, pp. 5219–5229, Jan. 2021.
- [37] C. Liu, X. Liu, D. W. K. Ng, and J. Yuan, "Deep residual learning for channel estimation in intelligent reflecting surface-assisted multi-user communications," *IEEE Trans. Wireless Commun.*, vol. 21, no. 2, pp. 898–912, Aug. 2022.
- [38] C. Liu, Z. Wei, D. W. K. Ng, J. Yuan, and Y.-C. Liang, "Deep transfer learning for signal detection in ambient backscatter communications," *IEEE Trans. Wireless Commun.*, vol. 20, no. 3, pp. 1624–1638, Nov. 2021.
- [39] J. Eargle, *Encode-Decode Noise Reduction (NR) Systems*. Boston, MA: Springer, 1992.
- [40] G. Hinton and T. J. Sejnowski, *Unsupervised learning: Foundations of neural computation*. Cambridge, MA: MIT press, 1999.
- [41] C. Zhang, D. Song, Y. Chen, X. Feng, C. Lumezanu, W. Cheng, J. Ni, B. Zong, H. Chen, and N. V. Chawla, "A deep neural network for unsupervised anomaly detection and diagnosis in multivariate time series data," in *Proc. AAAI Conf. Artif. Intell.*, Honolulu, HI, Jul. 2019.
- [42] L. Yang and A. Shami, "On hyperparameter optimization of machine learning algorithms: Theory and practice," *Neurocomputing*, vol. 415, pp. 295–316, Nov. 2020.
- [43] V. Dumoulin and F. Visin, "A guide to convolution arithmetic for deep learning," *arXiv:1603.07285v2*, Jan. 2018.
- [44] K. He and J. Sun, "Convolutional neural networks at constrained time cost," in *Proc. IEEE Conf. Comput. Vision. Pattern. Recogn.*, Boston, MA, Jun. 2015.
- [45] "TELAiRE HS30P relative humidity sensor," Available: <https://www.amphenol-sensors.com/en/component/edocman/viewdocument> Accessed: 2020-12-29.
- [46] "Chip temp. sensing NTC thermistor - SDNT series," Available: [http://www.sunlordinc.com/UploadFiles/PDF\\_Cat/20120507204152283.pdf](http://www.sunlordinc.com/UploadFiles/PDF_Cat/20120507204152283.pdf), Accessed: 2020-12-29.
- [47] P. Ali-Rantala, L. Ukkonen, L. Sydanheimo, M. Keskilammi, and M. Kivikoski, "Different kinds of walls and their effect on the attenuation of radiowaves indoors," in *Proc. IEEE Antennas Propag. Soc. Int. Symp.*, Columbus, OH, Jun. 2003.
- [48] "Code for engineering acceptance of generic cabling system," Guobiao Standards, GB/T GB/T50312-2016, 2016.
- [49] T. Lourenço, L. Matias, and P. Faria, "Anomalies detection in adhesive wall tiling systems by infrared thermography," *Constr. Build. Mater.*, vol. 148, pp. 419–428, Sep. 2017.
- [50] Y. Shi, Y. Wang, Y. Deng, H. Gao, Z. Lin, W. Zhu, and H. Ye, "A novel self-powered wireless temperature sensor based on thermoelectric generators," *Energy Convers. Manag.*, vol. 80, pp. 110–116, Apr. 2014.

- [51] NFPA, "Recommended practice for electrical equipment maintenance," National Fire Protection Association, Quincy, MA, Tech. Rep. NFPA-70-B, 2006.